学位論文

Live cell imaging studies on actin-based plant cell morphogenesis

アクチン繊維の可視化による高等植物細胞の形態形成・制御に関する研究

平成 20 年 12 月　博士（生命科学）申請

東京大学大学院新領域創成科学研究科

先端生命科学専攻

桧垣　匠

Live cell imaging studies on actin-based plant cell morphogenesis

Takumi Higaki

2008

Department of Integrated Biosciences,

Graduate School of Frontier Sciences,

The University of Tokyo

Acknowledgements

I first wish to express my deepest appreciation to Prof. Seiichiro Hasezawa (The University of Tokyo) for his guidance and encouragement throughout this study. I am also grateful to Dr. Toshio Sano (The University of Tokyo) and Dr. Natsumaro Kustuna (The University of Tokyo) for their instructions and support.

I thank to Prof. Noriaki Kondo (Teikyo University of Science and Technology), Prof. Kazuyuki Kuchitsu (Tokyo University of Science), Dr. Sachihiro Matsunaga (Osaka University), Dr. Hidetaka Kaya (Tokyo University of Science), Dr. Teruyuki Hayashi (National Institute of Agrobiological Sciences), Dr. Takamitsu Kurusu (Tokyo University of Science), Dr. Yasuhiro Kadota (RIKEN) and Dr. Tatsuaki Goh (Kobe University) for their critical advice and useful discussion.

I am grateful to Dr. Takatoshi Kagawa (Tsukuba University), Dr. Tsuyoshi Nakagawa (Shimane University), Prof. Roger Yonchien Tsien (University of California) and Prof. Ikuko Hara-Nishimura for the kind gift of 35S-sGFP(S65T)-mTn vectors, pGWB vectors, tdTomato vectors and transgenic tobacco BY-2 cell lines expressing SP-GFP-HDEL. I thank to Dr. Miyo Terao-Morita (Nara Instilute of Science and Technology) and Prof. Masao Tasaka (Nara Instilute of Science and Technology) for providing seeds of transgenic *Arabidopsis* expressing GFP-mTn.

I also appreciate the members of the Laboratory of Plant Cell Biology in Totipotency: Dr. Arata Yoneda, Dr. Yoko Tanaka, Dr. Masahide Ioki, Mr. Hidemasa Hoshino, Dr. Yoshihisa Oda, Mr. Yasunobu Otsuka, Ms. Yuko Kanazawa, Ms. Yuri Mitsui-Oda, Ms. Emiko Okubo-Kurihara, Ms. Tomomi Hayashi, Mr. Koichi Handa, Mr. Toshihisa Nomura, Ms. Asuka Inoue, Mr. Masanori Kenmochi, Ms. Atsuko Era, for their stimuli.

Finally, I want to thank my family and friends for their continuous support throught this study.

Contents

Abbreviations

2,4-D: 2,4-dichlorophenoxyacetic acid

3-D: three-dimensional

ABA: abscisic acid

ABD: actin binding domain

ADZ: actin depleted zone

AtFIM1: *Arabidopsis* fimbrin 1

BA: bistheonellide A

BDM: 2-3-butanedione monoxime

BY-2: Bright Yellow 2

CaMV: cauliflower mosaic-virus

CCD: charge coupled device

CD: cytochalasin D

CLSM: confocal laser scanning microscopy

DAPI: 4',6-diamidino-2-phenylindole

DIC: differential interference contrast

DMSO: dimethyl sulfoxide

ER: endoplasmic reticulum

FM4-64:

N-[3-triethylammoniumpropyl]-4-(6-(4-(diethylamino)phenyl)hexatrienyl)-pyridium dibromide

GFP: green fluorescent protein

JK: jasplakinolide

LatB: latrunculin B

LS: Linsmaier and Skoog

LSD: LS supplemented with 2,4-D

MBS: *m*-maleimidobenzoyl *N*-hydroxysuccinimide ester

MF: actin microfilament

MFTP: actin microfilament twin peaks

MIP: maximum intensity projection

MT: microtubule

mTn: mouse talin

PM: plasma membrane

PCR: polymerase chain reaction

RFP: red fluorescent protein

TIP: tonoplast intrinsic protein

TVM: tubular structure of vacuolar membrane

TVS: transvacuolar strand

VM: vacuolar membrane

General introduction

A plant body forms by the assembly of cells like a three-dimensional (3-D) jigsaw puzzle. Each cell piece is reproduced by cell division, and subsequently expands and acquires specific characteristics by differentiation. For example, in a leaf epidermal layer, a meristemoid mother cell divides into a neighboring cell and meristemoid. The neighboring cell rapidly expands and begins to play a major role in leaf growth. Meanwhile, the meristemoid differentiates into a pair of specialized cells called guard cells. The guard cells form a pore, called the stoma, which is essential for maintaining an appropriate level of gas and water vapor exchange between the plant and atmosphere. The guard cells regulate stomatal opening and closure. The accumulation and development of such cell types throughout morphogenesis finally produces a healthy plant.

During plant development, we can occasionally observe plant-specific mechanisms of changes in cell shape. Plant cells mainly display two characteristics concerning cell division: the division plane is determined before chromosomal separation in which the septum, called the cell plate, expands centrifugally so as to divide the parental cell into two. Cell enlargement is also a remarkable process in plant growth, and vacuoles play important roles in this step. In addition, differentiated plant cells (ex. guard cell, trichomes, root hair cells, pollen tubes) have notable cell shapes and properties. Of them, guard cells are particularly interesting in that they are able to swell and shrink in order to adapt to environmental changes. The question thus arises as to how these processes of plant cell morphogenesis are realized.

Actin is a ubiquitous protein of eukaryotic cells, and actin microfilaments (MFs) are formed from the physiological polymerization of actin molecules. MFs are a major component of the cytoskeleton and are involved in animal cell motility. As plant cells have a rigid cell wall and are generally immobile, the MFs are thought to generate the physical forces required for the various intracellular activities. Cytoplasmic streaming and organellar movement are excellent examples of

MF-dependent events in plants. Therefore, at the beginning of my research in the spring of 2004, I considered that actin was a promising candidate of a regulator of plant cell morphogenesis. At that time, there were already numerous methods for MF labeling, including treatment with fluorescently-labelled phalloidin or antibodies in fixed cells, the microinjection of these probes into living cells, and the expression of GFP-fusions to mammalian talin, an actin-binding protein. Although these techniques had contributed greatly to our earlier understanding of MF structures, they were insufficient for my interests because of their negative properties, such as artificial deformation and experimental limitations.

I therefore attempted to vitally visualize MFs in model plant cells with the minimal amount of cell damage, so as to elucidate the dynamics and roles of MFs in plant cell morphogenesis. In this study, I established an MF labeling method using an *Arabidopsis* actin side-binding protein, fimbrin 1 (AtFIM1), and analyzed the MF dynamics during cell division, vacuolar morphogenesis and also stomatal movement. In chapter I, I discovered a new distribution pattern of MF organization, which I termed actin microfilament twin peaks (MFTP), by expression of GFP fusions to the AtFIM1 actin binding domain 2 (ABD2) in tobacco BY-2 cells. The position of the MFTP valley was coincident with the future division plane, and pharmacological perturbations of the MFTP structures resulted in the formation of an oblique cell wall, suggesting the importance of the MFTP in determination of the cell division plane. In chapter II, I analyzed the contribution of MFs to cell plate formation. Time-sequential observations revealed that the MFs gradually accumulated near the cell plate and that MF-disruption caused a slowdown of cell plate expansion. Furthermore, MF-disruption was found to impair endosome movement and endoplasmic reticulum recruitment near the expanding cell plate, suggesting that MFs contribute to cell plate expansion via regulation of the endomembrane systems. In chapter III, I examined the spatio-temporal interaction between MFs and vacuoles in interphase tobacco BY-2 cells. The majority of MFs localized to the vacuolar membranes, and was essential for maintenance of the vacuolar structures. In chapter IV, I visualized the MFs in guard cells by expressing GFP-ABD2 in

Arabidopsis thaliana. I also developed quantitative evaluation methods for understanding MF configurations using microscopic image processing techniques. Based on these microscopic observations and quantitative analyses, I found that MFs were transiently bundled in the process of diurnal stomatal opening. In addition, I found that excessive MF-bundling, resulting from continuously induced GFP-mTn expression, suppressed stomatal opening. These results suggested the importance of MF bundle dissociation in the promotion of stomatal opening.

Based on these series of studies, I finally discuss the importance of MF interactions with membranous structures in actin-based plant cell morphogenesis.

Chapter I: Determination of cell division plane

Abstract

In this chapter, I established a tobacco BY-2 cell line, stably transformed with a GFP-AtFIM1 actin-binding domain 2 (ABD2) construct, that allows visualization of actin microfilaments (MFs) in living cells. Using this cell line, designated BY-GF11, I performed time-sequential observations of MF dynamics during cell cycle progression. Detailed analyses revealed the appearance of a broad MF band in the late G2 phase that separated to form a structure corresponding to the so-called actin-depleted zone (ADZ) in mitosis. In BY-GF11 cells, the MF structure at the cell cortex in mitosis appeared to form two bands rather than the ADZ. Measurements of fluorescent intensities of the cell cortex indicated an MF distribution that resembled two peaks, and I therefore named the structure MF 'twin peaks' (MFTP). The division plane formed exactly within the valley between the MFTP at cytokinesis, and this division plane was distorted by disruption of the MFTP by an inhibitor of actin polymerization. These results suggest that the MFTP originates from the broad MF band in the G2 phase and functions as a marker of cell division plane.

Introduction

In numerous studies, the actin microfilaments (MFs) of different plant cell types has been visualized by fluorescent-phalloidin labelling or immunostaining after fixation. However, because of the difficulties in preserving the integrity of the MFs, due to their sensitivity to the chemical fixation treatments, such post-fixation staining methods appear to generate artificial MF rearrangements. An alternative approach to observing MFs, which negates the need for fixation, is the microinjection of fluorescent-labelled phalloidin. Using this technique, the dynamic redistribution of MFs during mitosis and cytokinesis have been clarified *in vivo* in *Haemanthus* endosperm cells (Schmit and Lambert 1990) and in *Tradescantia* stamen hair cells and stomatal complexes (Cleary 1995, Cleary et al. 1992, Zhang et al. 1993). However, drawbacks of this technique include the brevity of the observation period due to the diffusion of fluorescence into vacuoles and adjacent cells, and the fact that not all plant cell types are amenable to microinjection. In contrast, recent molecular techniques employing the green fluorescent protein (GFP) have enabled us to visualize MFs *in vivo*. Direct labelling of actin with GFP has demonstrated MFs in yeast and *Dictyostelium* (Doyle and Botstein 1996, Aizawa et al. 1997), although expression of GFP-actin was found to inhibit cellular activities in *Dictyostelium* cells (Aizawa et al. 1997). An alternative to direct labelling is the labelling of proteins with actin-binding domains (ABDs). GFP fusion to a mouse talin (mTn) actin-binding domain labelled the MFs in tobacco BY-2 cells following particle bombardment, and also those in stably transformed *Arabidopsis* plants (Kost et al. 1998). By using the fusion of mTn to the fluorescent protein, MF dynamics were well described in pollen tubes and trichomes of *Arabidopsis* plants (Brembu et al. 2004, Kost et al. 1998, Mathur et al. 1999, Saedler et al. 2004). Although no time-sequential imaging of cell cycle progression was performed, GFP fusion with the ABD of fimbrin also labelled MFs in tobacco protoplasts and BY-2 cells, *Arabidopsis* and *Medicago* cells (Sheahan et al. 2004a,b).

During cell cycle progression, a dynamic change in the MFs has been

demonstrated by fluorescent-phalloidin labelling, after fixation or by microinjection, in various plant cell types such as *Allium*, tobacco BY-2 and *Tradescantia* stamen hair cells (Cleary et al. 1992, Hasezawa et al. 1991, Liu and Palevitz 1992, Mineyuki and Palevitz 1990). These reports described two main MF structures from the G2 phase to mitosis: one constitutes the actin band that co-localizes with, but is wider than, the microtubule preprophase band, which is in alignment with the future division plane (Liu and Palevitz 1992, Mineyuki 1999); the other is the so-called actin depleted zone (ADZ) that appears in late G2 to mitosis (Cleary et al. 1992, Liu and Palevitz 1992). Although the ADZ has been proposed to determine the position of the cell division plane (Cleary 1995, Hoshino et al. 2003), the exact relationship between the broad actin band, the ADZ and division plane has not yet been clarified because of difficulties associated with time-sequential observations in fixed or microinjected cells.

In this chapter, I established a tobacco BY-2 cell line, stably transformed with a GFP-ABD2 construct, that allows visualization of MFs in living cells without the need for fixation. Using this cell line, designated BY-GF11, I performed time-sequential observations of MF dynamics during cell cycle progression. Detailed observations revealed that the broad MF band observed in the late G2 phase separated into two MF bands that were quite similar to the ADZ at mitosis, and that a division plane formed between these two MF bands during cytokinesis. My results demonstrate that the two MF bands that appear in mitosis originate from the broad MF band in the late G2 phase, and are involved in determination of the division plane.

Methods

Plant material and synchronization

Tobacco BY-2 (*Nicotiana tabacum* L. cv. Bright Yellow 2) suspensions were diluted 95-fold with a modified Linsmaier and Skoog medium supplemented with 2,4-D (LSD medium) at weekly intervals, as described by Nagata et al. (1992). The

cell suspensions were agitated on a rotary shaker at 130 rpm at 27°C in the dark. Cell synchronization was performed as described by Nagata et al. (1992). In brief, 10 ml 7-day-old cells were transferred to 95 ml fresh medium and cultured for 24 hours with 5 mg l^{-1} aphidicolin (Sigma, St Louis, MO, USA). The cells were washed with 10 vol fresh medium and then resuspended in the same medium. After aphidicolin release, cell cycle progression was monitored by counting the percentage of cells in mitosis (mitotic index), which was determined with a fluorescence microscope after staining the nuclei with 20 $\mu g l^{-1}$ 4', 6-diamidino-2-phenylindole (DAPI).

Construction of GFP-ABD2

The region encoding the second actin-binding domain (ABD2; amino acids 325-687) of AtFim1 (McCurdy and Kim 1998) was PCR amplified from an *Arabidopsis thaliana* cDNA library. The amplified fragment replaced the mTn of the CaMV 35S-sGFP (S65T)-mTn vector, kindly provided by Dr T. Kagawa of Tsukuba University, resulting in an in-frame fusion of N-terminus GFP and C-terminus fimbrin ABD2. The 35S-sGFP(S65T)-mTn vector was modified from the 35S-sGFP (S65T) vector, obtained from Dr Y. Niwa of Shizuoka Prefecture University, so as to contain 6 × Gly-Ala repeats between GFP and the mTn. The resulting 35S-sGFP (S65T)-fimbrin ABD2 region was then subcloned into the pCAMBIA1300 binary vector (CAMBIA, Canberra, Australia) for transformation.

Transformation and establishment of the BY-2 cells stably expressing GFP-ABD2

The GFP-ABD2 construct was transformed into *Agrobacterium tumefaciens* strain, LBA4404. A 4 ml aliquot of 3-day-old BY-2 cells was incubated with 100 µl overnight culture of the transformed *A. tumefaciens* as described by An (1985). After 2 days' incubation at 27°C, cells were washed four times in 5 ml LSD medium, then plated onto solid LSD medium containing 500 mg l^{-1} carbenicillin and 15 mg l^{-1} hygromycin. Calluses, which appeared after 20 days, were transferred onto new plates and cultured independently until they reached approximately 1 cm in

diameter, when they were transferred to 20 ml liquid LSD medium and agitated on a rotary shaker at 130 rpm at 27°C in the dark. After 1 month a cell line suitable for observing MFs was selected by examination of GFP-fluorescence by fluorescent microscopy, and the cell line obtained was designated BY-GF11. Transformation of cell suspensions of *Arabidopsis* Col-0 was performed essentially as described by Oda et al. (2005) with the same GFP-ABD2 construct.

Transient expression

A cell suspension of 3-day-old BY-2 cells was filtrated onto filter paper, and the cells bombarded with gold particles (1.0 μm) coated with the appropriate vector constructs using a particle-delivery system (PDS-1000/He, Bio-Rad, Hercules, CA, USA) according to the manufacturer's recommendations. Filtrated BY-2 cells were placed at a distance of 6 cm under the stopping screen and bombarded in a vacuum of 28 inches Hg at a helium pressure of 1100 psi. Following bombardment, cells were diluted in LSD medium and kept in the dark at 27°C for 6-12 hours before observation.

Cell staining

For simultaneous observations of rhodamine-phalloidin and GFP-ABD2, the BY-GF11 cells were suspended in a solution containing 50 mM PIPES (pH 6.8), 1 mM $MgSO_4$, 5 mM EGTA, 1-5% glycerol, 150 mM mannitol and 0.07 μM rhodamine-phalloidin (Molecular Probes, Eugene, OR, USA) and incubated for 30 min at room temperature. For observing the division planes, cells were stained with 0.05% aniline blue (Biosupplies Australia, Parkville, Victoria, Australia) for 15 min.

To simultaneously observe the plasma membrane (PM) and vacuolar membrane (VM) in BY-GF11 cells, *N*-[3-triethylammoniumpropyl]-4-(6-(4-(diethylamino)phenyl)hexatrienyl)-pyridium dibromide (FM4-64; Molecular Probes) was added to the cell suspension at a final concentration of 16 μM. The cells were incubated for 2 min, diluted to 1:32 in fresh

culture medium, and observed 10 hours after the FM4-64 addition.

Microscopy

For time-sequential observations, synchronized BY-GF11 cells were transferred into 35-mm-diameter Petri dishes with 14-mm-diameter coverslip windows at the bottom (Matsunami Glass Ind. Ltd, Osaka, Japan). The dishes were placed onto the inverted platform of a fluorescence microscope (IX-70; Olympus) equipped with a confocal laser scanning head and control systems (CLSM GB-200; Olympus, Tokyo, Japan) or a cooled CCD camera head system (Cool-SNAP HQ; PhotoMetrics, Huntington Beach, Canada). Maximum intensity projections were reconstructed from the continuous optical sections within a 0.5-μm step size using MetaMorph software (Universal Imaging, Downingtown, PA, USA). Indirect quantification of fluorescence levels was performed using ImageJ software (Abramoff et al. 2004).

Results

Visualization of actin microfilaments by stable GFP-ABD2 expression

The second actin-binding domain (ABD2) of the *Arabidopsis* AtFim1 protein was fused to the C-terminus of GFP and stably expressed in tobacco BY-2 cells to generate the BY-GF11 (BY-2 cells stably expressing GFP-ABD2 line 11) cell line. Confocal observations revealed GFP fluorescence of filamentous structures near the cell cortex (Fig. I-1A) and along the transvacuolar strands (TVSs) at the mid-plane (Fig. I-1B; see also chapter III for detail.). Such filamentous structures were also observed in another cell line of BY-GF8 transformed with the same construct (see Fig. I-5). These cortical filamentous structures closely resembled those observed in cells following particle bombardment with the mouse talin MF-binding domain (GFP-mTn) (Fig. I-1C; Kost et al. 1998), although the MF structures in the TVSs could not be clearly observed in the GFP-mTn-bombarded cells (Fig. I-1D). *Arabidopsis* cell cultures stably expressing GFP-ABD2 also revealed similar

filamentous structures near the cell cortex and in the cytoplasm (Fig. I-1E, F). To ensure the GFP-labelled fluorescent structures of the BY-GF11 cells did represent MFs, rhodamine-phalloidin staining was performed after gentle permeabilization of the cells with glycerol. The structures labelled by GFP and rhodamine fluorescence almost overlapped at both the cell cortex and the cell mid-plane (Fig. I-1G, H, I, J, K, L). In addition, the GFP fluorescence disappeared following treatment with 100 μM cytochalasin D (CD), an inhibitor of actin polymerization (see Fig. I-8). These observations clearly indicate that the GFP-ABD2 fusion protein labelled MFs in the tobacco BY-GF11 cells.

Cortical and cytoplasmic MF organization in interphases of living tobacco BY-2 cells

As the MF structures were shown to be dynamically changing during cell cycle progression in fixed cells, I first monitored the changes in MF structures in living BY-GF11 cells. At the G1 phase, transverse and meshwork-like MFs were observed at the cell cortex (Fig. I-2A), as also found in rhodamin-phalloidin-stained BY-2 cells after fixation (Hasezawa et al. 1991). At the mid-plane, the MFs extended through the cytoplasm from the cell nucleus to the cell periphery (Fig. I-2B). A maximum intensity projection (MIP) image showed a basket-like MF structure within a whole cell (Fig. I-2C). At S phase, when the cell nucleus moved from the cell periphery to the centre, the MFs extended radially from the nuclear surface to the cell periphery (Fig. I-2E, F). In the G2 phase, the cortical MFs became predominantly transverse-oriented and concentrated at the cell centre so as to form a band-like structure (Fig. I-2G, I). At the mid-plane, there was an increase in the amount of GFP fluorescence surrounding the cell nucleus and at the mid-region of the cell cortex (Fig. I-2H).

Cortical MFs in the G2 phase separated in mitosis

Subsequent observation of MF structures during mitosis revealed that the cortical MFs that were transversely oriented at the G2 phase formed meshwork structures at metaphase (Fig. I-2J). At the centre of the cell, a zone with a weak

MF network but still with some MFs localized could be distinguished (Fig. I-2L, arrow). This structure closely resembled the ADZ, although in the BY-GF11 cells there appeared to be two MF bands (Fig. I-2L, asterisks) rather than the ADZ. By cell staining with the fluorescent dye, FM4-64 (Kustuna and Hasezawa 2002, Bolte et al. 2004, Samaj et al. 2005; see also chapter II and III.), it was revealed that the two band-like MF structures were mainly localized on the PM rather than the VM (Fig. I-3). At the mid-plane, the MFs stretched throughout the cytoplasm as in the G1 through G2 phases, but the filaments were now very fine (Fig. I-2K). Only a dim fluorescence was observed in the mitotic apparatus. In late anaphase, two populations of longitudinal MFs appeared temporally between the two sets of chromosomes (Fig. I-2N; see chapter II for detail.), as reported in rhodamine-phalloidin injected *Tradescantia* cells (Cleary et al. 1992). In telophase, the MFs localized at the edges of the expanding septum termed cell plate (Fig. I-2Q, R; see chapter II for detail.).

The above-mentioned MF dynamics could be observed in a single living cell by time-sequential observations from late G2 through mitosis to cytokinesis. In the late G2 phase, the cortical MF band could be recognized at the centre of the cell (Fig. I-4A). As the cell cycle progressed, a zone with weak MFs appeared at the centre of the cortical MF band (Fig. I-4B, C), then two MF bands became evident at mitosis (Fig. I-4D, E, F). After cytokinesis, the division plane seemed to form at the site of the weak MFs in mitosis (Fig. I-4I).

As the above time-sequential observations at the mid-plane by confocal laser scanning microscopy (CLSM) suggested a separation of the cortical MF band from the late G2 phase to mitosis, I attempted to observe the dynamics of the cortical MF structures in more detail. The MF band was observed in the late G2 phase, when a thick cytoplasmic disc-like structure at the center of the cell could be clearly distinguished by a differential interference contrast (DIC) image obtained from light microscopy (Fig. I-5A, E). As the cell cycle progressed to mitosis, the MF band began to separate at the cell cortex, and a zone with a weak cortical MF network appeared at the centre of the MF band (Fig. I-5F, G, H). Measurements of

fluorescent intensity at the cell cortex by fluorescent microscopy showed the highest intensity at the centre of the cell in the late G2 phase (Fig. I-5I). With cell cycle progression, the fluorescent intensity at the cell centre decreased (Fig. I-5J) and resulted in the appearance of two peaks together with an increase in the distance between the MF bands (Fig. I-5K, L). In accordance with the reduced fluorescent intensity at the cell centre, the thick cytoplasmic disc-like structure became obscure (Fig. I-5D). Based on the distribution of fluorescent intensities of the cortical MF structures in mitosis, I named the structure composed of the two MF bands as the MF 'twin peaks' (MFTP). This MFTP structure was confirmed in another cell line of BY-GF8 and in BY-2 cells incubated with rhodamine-phalloidin after permeabilization (Fig. I-5M, N, O, P, Q, R).

A time-sequential observation at the cell surface also revealed the separation of the MF band (Fig. I-6). In the late G2 phase, MFs that were transversely oriented (Fig. I-6B) started to develop a meshwork structure and subsequently formed two MF bands with a weak MF network zone in mitosis (Fig. I-6H).

Relationship of MFTP and division plane determination

Continuation of the time-sequential observations demonstrated that the division plane was formed 120 min from the G2 phase (Fig. I-7A, B). The division plane appeared to develop at the position previously occupied by the zone with a weak MF network in metaphase (Fig. I-7C). Measurement of the distances between the two peaks of the MFTP at mitosis, and also of that between one peak and the division plane, indicated that the latter was almost half the distance of the former (Fig. I-7D, E), and suggested that the division plane was inserted in the valley of the MFTP.

To investigate the functional relevance of the MFTP to the division plane determination, I examined an effect of CD, an inhibitor of actin polymerization. When I applied 100 μM CD 6 hours after aphidicolin removal, the MF structures disappeared in 2 hours (Fig. I-8A). Although cell cycle progression was not affected by the CD treatment (Fig. I-8B), abnormal division planes were observed 11 hours

after aphidicolin removal by aniline blue staining (Fig. I-8E). In the non-treated control cells the division planes were smooth and sharp, while in the CD treated cells some were not vertical to the cell cortex and some were broad and twisted. Removal of the CD at 8 hours restored the MF structures, but the division plane was still twisted (Fig. I-8A, E). These 'distorted' division planes were observed for approximately 30% of the cells treated with CD from 6 to 8 hours, in which the cells with MFTP were mostly observed (Fig. I-8C, D). In contrast, in cells treated with CD from 9 to 11 hours, in which phragmoplasts that are structures sandwiching the developing cell plate (see chapter II for detail.), were mostly observed, the percentage of distorted division planes decreased significantly (Fig. I-8C, D).

Discussion

Establishment of tobacco BY-GF cell line

In this study I established a tobacco BY-GF11 cell line expressing a GFP-ABD2 fusion protein through which MFs could be visualized, and the MF dynamics during cell cycle progression could be observed. In previous studies, an GFP-mTn was most commonly used to visualize MFs in living cells (Kost et al. 1998). My transient expression analyses using particle-bombarded GFP-mTn revealed the presence of cortical MFs, but no clear cytoplasmic MF structures could be observed (Fig. I-1C, D). Although GFP-ABD2 is recognized as a more reliable MF-marker than GFP-mTn (Sheahan et al. 2004b, Ketelaar et al. 2004, Higaki et al. 2007), recent studies have shown that overexpression of GFP-ABD2 can cause growth inhibition of pollen tubes (Kathleen et al. 2004) and organelle motility (Holweg 2007), suggesting the need for care and attention in the use of such GFP markers. My BY-GF11 cells that stably express the GFP-ABD2 fusion protein clearly show the MF structures, including those within TVSs, during cell cycle progression. The BY-GF11 cells grow as well as non-transformed tobacco BY-2 cells, and show a cell synchrony of approximately 50% of the mitotic index after aphidicolin removal (Fig. I-8B), indicating their minimal side effects.

Fimbrin is an actin side-binding protein, and the first plant fimbrin-like gene, *AtFIM1*, was identified in *Arabidopsis* (McCurdy and Kim, 1998). Whereas GFP fusions with the full-length AtFim1 protein, or with the amino terminus of the ABD1, did not show clear MF structures (Sheahan et al. 2004b, Wang et al. 2004), fusions with the fimbrin ABD2 enabled visualization of MFs in tobacco protoplasts and BY-2 cells, *Arabidopsis*, and also *Medicago* cells (Sheahan et al. 2004a,b, Wang et al. 2004, Voigt et al. 2005). My BY-GF11 cell line, expressing a GFP-ABD2 fusion protein, also successfully allowed visualization of MFs. Moderate binding activity of the fimbrin ABD2 to MFs was suggested to provide a non-invasive level of MF labelling (Sheahan et al. 2004b). My observation that the GFP fluorescence of BY-GF11 cells could be maintained only after treatment with a low concentration of glycerol to gently permeabilize the PM (Fig. I-1G, H) supports the affinity of the fimbrin ABD2 for MFs.

The MF structures observed in BY-GF11 cells were essentially similar to those visualized in tobacco BY-2 cells with fluorescent phalloidin after fixation (Hasezawa et al. 1991, Hoshino et al. 2003). Rhodamine-phalloidin labelling is thought to bundle the MFs: thick MFs were often observed, especially without treatment with *m*-maleimidobenzoyl *N*-hydroxysuccinimide ester (MBS), a potent protein bridging reagent (Hasezawa et al. 1989, Sonobe and Shibaoka, 1989). In contrast, thick MFs were observed in the BY-GF11 cells from G1 to S phase, whereas very fine MFs were identified from G2 to mitosis. Although the precise role of these thick and fine MFs has yet to be clarified, the fine MFs could be visualized with GFP-ABD2 without rhodamine-phalloidin labelling.

Formation of MFTP and its role in the division plane determination

The BY-GF11 cell line allowed me to observe the time-sequential dynamics of MFs, and revealed a separation of the cortical MF band from the late G2 phase (Figs I-4, I-5, I-6). Changes in distribution of the relative fluorescence intensity at the cell cortex showed this separation clearly (Fig. I-5I, J, K, L), and allowed me to identify the resulting MF structure which I termed the MFTP. The separation

formed two MF bands, together with a region of weak GFP fluorescence that closely resembled the so-called ADZ. Observations of the BY-GF11 cells showed the cortical MFs to be distributed only in the central region, and apparently to form two bands. Although the relationship between the cortical MF bands appeared at G2 phase and ADZ has not been completely addressed, Mineyuki (1999) suggested the appearance of an ADZ from the cortical MF band. My observations of a living cell clearly demonstrated that the cortical MF band was the origin of the MFTP, and that the valley between the peaks closely resembled the ADZ. Moreover, the MFs in the cortical MF band at the G2 phase were mainly transverse-oriented, whereas those after separation showed meshwork-like structures (Fig. I-6). These MF structures therefore appear to have been formed not by a simple separation and movement of the transverse cortical MFs, but rather by some rearrangement of the MF networks.

The ADZ has been suggested to function as a marker of division plane after disruption of microtubule preprophase band (Cleary, 1995, Hoshino et al. 2003), and my time-sequential observations further suggest that the site of the division plane corresponds to the valley of the MFTP (Fig. I-7C, E). Measurements of fluorescent intensities of cortical MFs strongly support the above observation. The increased number of cells with a distorted division plane by disruption of the MFTP suggested its role in proper determination of the division plane (Fig. I-8D).

Interestingly, disruption of the actin phragmoplast had little effect on determination of division plane (Fig. I-8C, D). These results suggest that, in telophase, the MF structures were not necessary for cell division plane determination. I will discuss the roles of MFs in telophase in chapter II.

In conclusion, I have established a tobacco BY-GF11 cell line that expresses GFP-ABD2 and allows visualization of the MF structures. Live cell imaging demonstrated the appearance of MFTP, which formed a valley closely resembling the ADZ, and which originated from the cortical MF band in the late G2 phase. Subsequent division plane formation at exactly the site occupied by the MFTP valley at mitosis further strengthens the proposed role of MFTP in determining the division site.

References

Abramoff MD, Magelhaes PJ, Ram SJ. (2004) Image processing with ImageJ. *Biophoto. Int.* 11:36-42.

Aizawa H, Sameshima M Yahara I. (1997) A green fluorescent protein-actin fusion protein dominantly inhibits cytokinesis, cell spreading, and locomotion in *Dictyostelium. Cell Struct. Funct.* 22:335-345.

An G. (1985) High efficiency transformation of cultured tobacco cells. *Plant Physiol.* 79:568-570.

Bolte S, Talbot C, Boutte Y, Catrice O, Read ND, Satiat-Jeunemaitre B. (2004) FM-dyes as experimental probes for dissecting vesicle trafficking in living plant cells. *J. Microscopy* 214:159-173.

Brembu T, Winge P, Seem M, Bones AM. (2004) NAPP and PIRP encode subunits of a putative Wave regulatory protein complex involved in plant cell morphogenesis. *Plant Cell* 16:2335-2349.

Cleary AL. (1995) F-actin redistributions at the division site in living Tradescantia stomatal complexes as revealed by microinjection of rhodamine-phalloidin. *Protoplasma* 185:152-165.

Cleary AL, Gunning BES, Wasteneys GO, Hepler PK.(1992) Microtubule and F-actin dynamics at the division site in living Tradescantia stamen hair cells. *J. Cell Sci.* 103:977-988.

Doyle T, Botstein D. (1996) Movement of yeast cortical actin cytoskeleton visualized *in vivo. Proc. Natl Acad. Sci. USA* 93:3886-3891.

Hasezawa S, Hogetsu T, Syono K. (1989) Changes of actin filaments and cellulose fibrils in elongating cells derived from tobacco protoplasts. *J. Plant Physiol.* 134:115-119.

Hasezawa S, Marc J, Palevitz BA. (1991) Microtubule reorganization during the cell cycle in synchronized BY-2 tobacco suspensions. *Cell Motil. Cytoskel.* 18:94-106.

Higaki T, Sano T, Hasezawa S. (2007) Actin microfilament dynamics and actin side-binding proteins in plants. *Curr. Opin. Plant Biol.* 10:549-556.

Holweg CL. (2007) Living markers for actin block myosin-dependent motility of plant organelles and auxin. *Cell Motil. Cytoskel.* 64:69-81.

Hoshino H, Yoneda A, Kumagai F, Hasezawa S. (2003) Roles of actin-depleted zone and preprophase band in determining the division site of higher-plant cells, a tobacco BY-2 cell line expressing GFP-tubulin. *Protoplasma* 222:157-165.

Kathleen LW, Lovy-Wheeler A, Voigt B, Menzel D, Kunkel JG, Hepler PK. (2006) Imaging the actin cytoskeleton in growing pollen tubes. *Sex. Plant Reprod.* 19:51-62.

Ketelaar T, Anthony RG, Hussey PJ. (2004) Green fluorescent protein-mTalin causes defects in actin organization and cell expansion in Arabidopsis and inhibits actin depolymerizing factor's actin depolymerizing activity *in vitro*. *Plant Physiol.* 136:3990-3998.

Kost B, Spielhofer P, Chua NH. (1998) A GFP-mouse talin fusion protein labels plant actin filaments *in vivo* and visualize the actin cytoskeleton in growing pollen tubes. *Plant J.* 16:393-401.

Kutsuna N, Hasezawa S. (2002) Dynamic organization of vacuolar and microtubule structures during cell cycle progression in synchronized tobacco BY-2 cells. Plant Cell Physiol. 43:965-973.

Kutsuna N, Kumagai F, Sato MH, Hasezawa S. (2003) Three-dimensional reconstruction of tubular structures of vacuolar membrane throughout mitosis in living tobacco cells. *Plant Cell Physiol.* 44:1045-1054.

Liu B, Palevitz BA. (1992) Organization of cortical microfilaments in dividing root cells. *Cell Motil. Cytoskel.* 23:252-264.

Mathur J, Spielhofer P, Kost B, Chua NH. (1999) The actin cytoskeleton is required to elaborate and maintain spatial patterning during trichome cell morphogenesis in *Arabidopsis thaliana*. *Development* 126:5559-5568.

McCurdy DW, Kim M. (1998) Molecular cloning of a novel fimbrin-like cDNA from *Arabidopsis thaliana*. *Plant Mol. Biol.* 36:23-31.

Mineyuki Y. (1999) The preprophase band of microtubules: its function as a cytokinetic apparatus in higher plants. *Int. Rev. Cytol.* 187:1-49.

Mineyuki Y, Palevitz BA. (1990) Relationship between preprophase band organization, F-actin and the division site in *Allium*. *J. Cell Sci.* 97:283-295.

Nagata T, Nemoto Y, Haswzawa S. (1992) Tobacco BY-2 cell line as the 'HeLa' cell in the cell biology of higher plants. *Int. Rev. Cytol.* 132:1-30.

Oda Y, Mimura T, Hasezawa S. (2005) Regulation of secondary cell wall development by cortical microtubules during tracheary element differentiation in *Arabidopsis* cell suspensions. *Plant Physiol.* 137:1027-1036.

Saedler R, Mathur N, Srinivas BP, Kernebeck B, Hülskamp M, Mathur J. (2004) Actin control over microtubules suggested by DISTORTED2 encoding the Arabidopsis ARPC2 subunit homolog. *Plant Cell. Physiol.* 45:813-822.

Samaj J, Read ND, Volkmann D, Menzel D, Baluska F. (2005) The endocytic network in plants. *Trends Cell Biol.* 15:425-433.

Schmit AC, Lambert AM. (1990) Microinjected fluorescent phalloidin *in vivo* reveals the F-actin dynamics and assembly in higher plant mitotic cells. *Plant Cell* 2:129-138.

Sheahan MB, Rose RJ, McCurdy DW. (2004a) Organelle inheritance in plant cell division: the actin cytoskeleton is required for unbiased inheritance of chloroplasts, mitochondria and endoplasmic reticulum in dividing protoplasts. *Plant J.* 37:379-390.

Sheahan MB, Staiger CJ, Rose RJ, McCurdy DW. (2004b) A green fluorescent protein fusion to actin-binding domain 2 of Arabidopsis fimbrin highlights new features of a dynamic actin cytoskeleton in live plant cells. *Plant Physiol.* 136:3968-3978.

Sonobe S, Shibaoka H. (1989) Cortical fine actin filaments in higher plant cells visualized by rhodamine-phalloidin after pretreatment with m-maleimidobenzoyl N-hydroxysuccinimide ester. *Protoplasma* 148:80-86.

Voigt B, Timmers AC, Samaj J, Hlavacka A, Ueda T, Preuss M, Nielsen E, Mathur J, Emans N, Stenmark H, Nakano A, Baluska F, Menzel D. (2005) Actin-based motility of endosomes is linked to the polar tip growth of root hairs. *Euro. J. Cell Biol.* 84:609-621.

Wang YS, Motes CM, Mohamalawari DR, Blancaflor EB. (2004) Green fluorescent protein fusions to Arabidopsis fimbrin 1 for spatio-temporal imaging of F-actin dynamics in root. *Cell Motil. Cytoskel.* 59:79-93.

Zhang D, Wadsworth P, Hepler PK. (1993) Dynamics of microfilaments are similar, but distinct from microtubules during cytokinesis in living, dividing plant cells. *Cell Motil. Cytoskel.* 24:151-155.

Figures

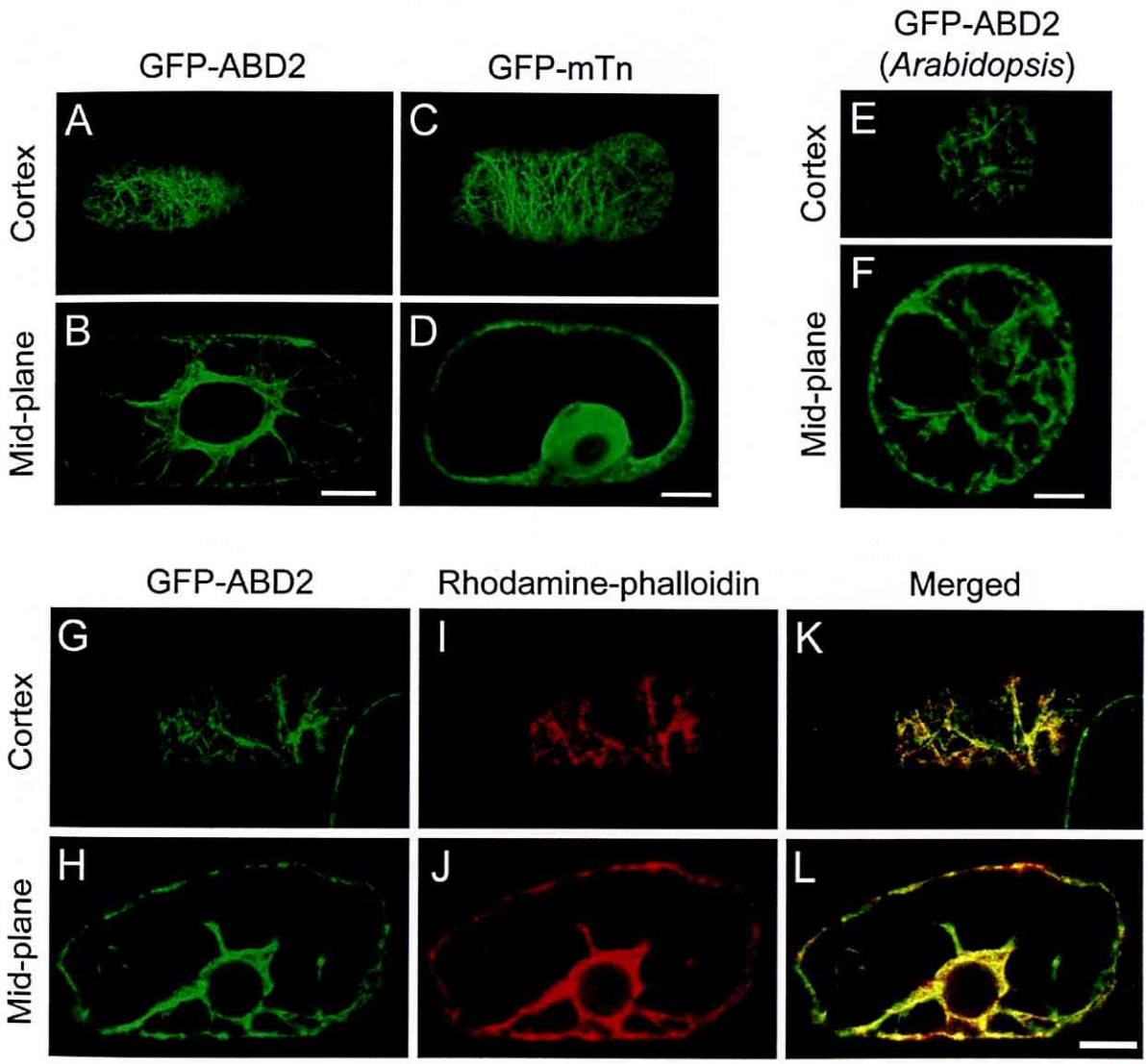

Figure I-1. Visualization of microfilaments in tobacco BY-2 cells and an *Arabidopsis* cell culture. MFs visualized in tobacco BY-2 cells stably expressing GFP-ABD2 (A, B); transiently expressing GFP-mTn (C, D); and in an *Arabidopsis* cell culture stably expressing GFP-ABD2 (E, F). Co-localization of GFP (G, H) and rhodamine-phalloidin (I, J) fluorescence in a permeabilized BY-GF11 cell, and their merged fluorescences (K, L). Scale bars: 10 μm.

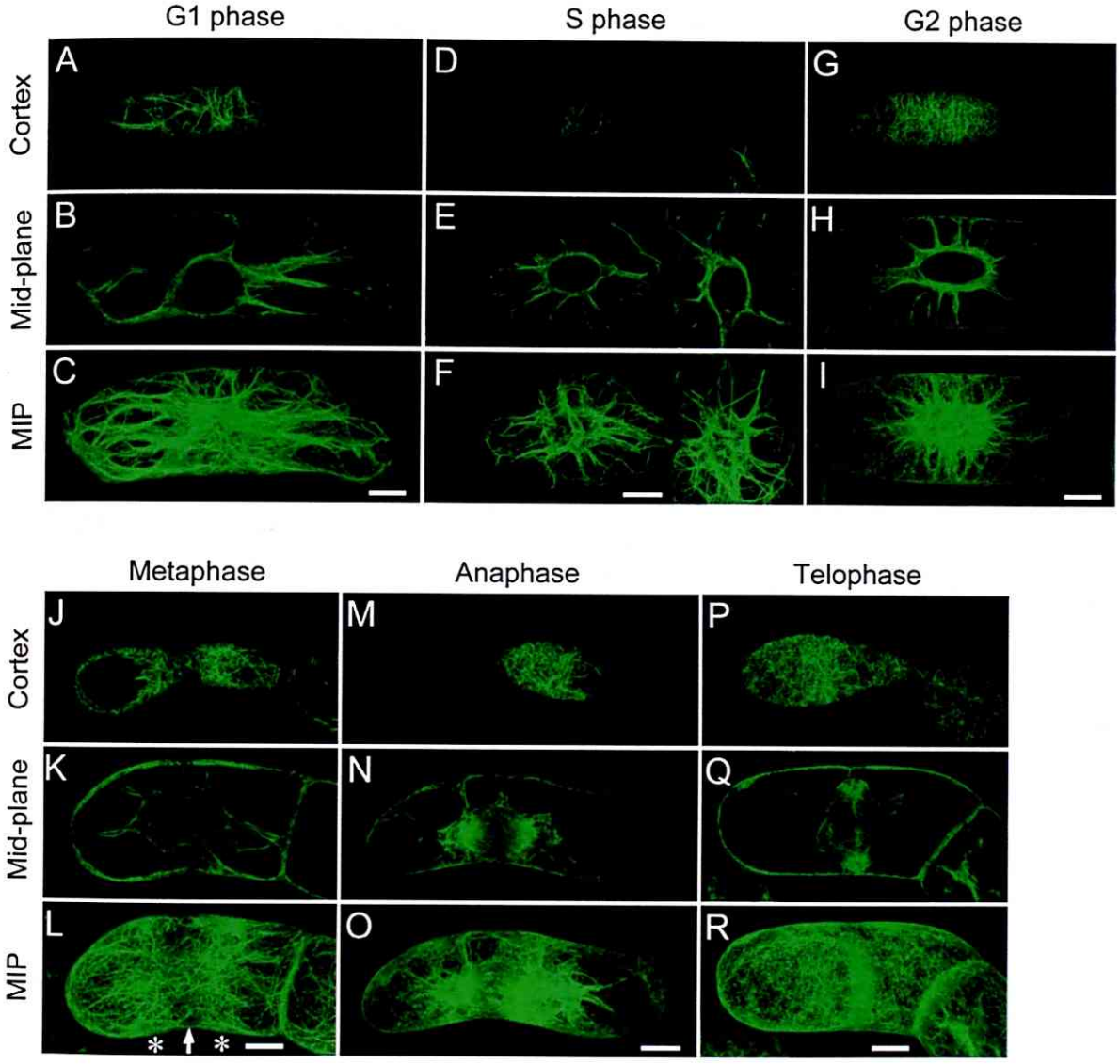

Figure I-2. Dynamics of MFs during cell cycle progression. BY-GF11 cells were observed in the G1 (A, B, C), S (D, E, F), G2 (G, H, I), metaphase (J, K, L), anaphase (M, N, O) and telophase (P, Q, R). MIP stands for maximum intensity projection. (L) Asterisks and arrow show MF bands and a zone with a weak MF network, respectively. Scale bars: 10 μm.

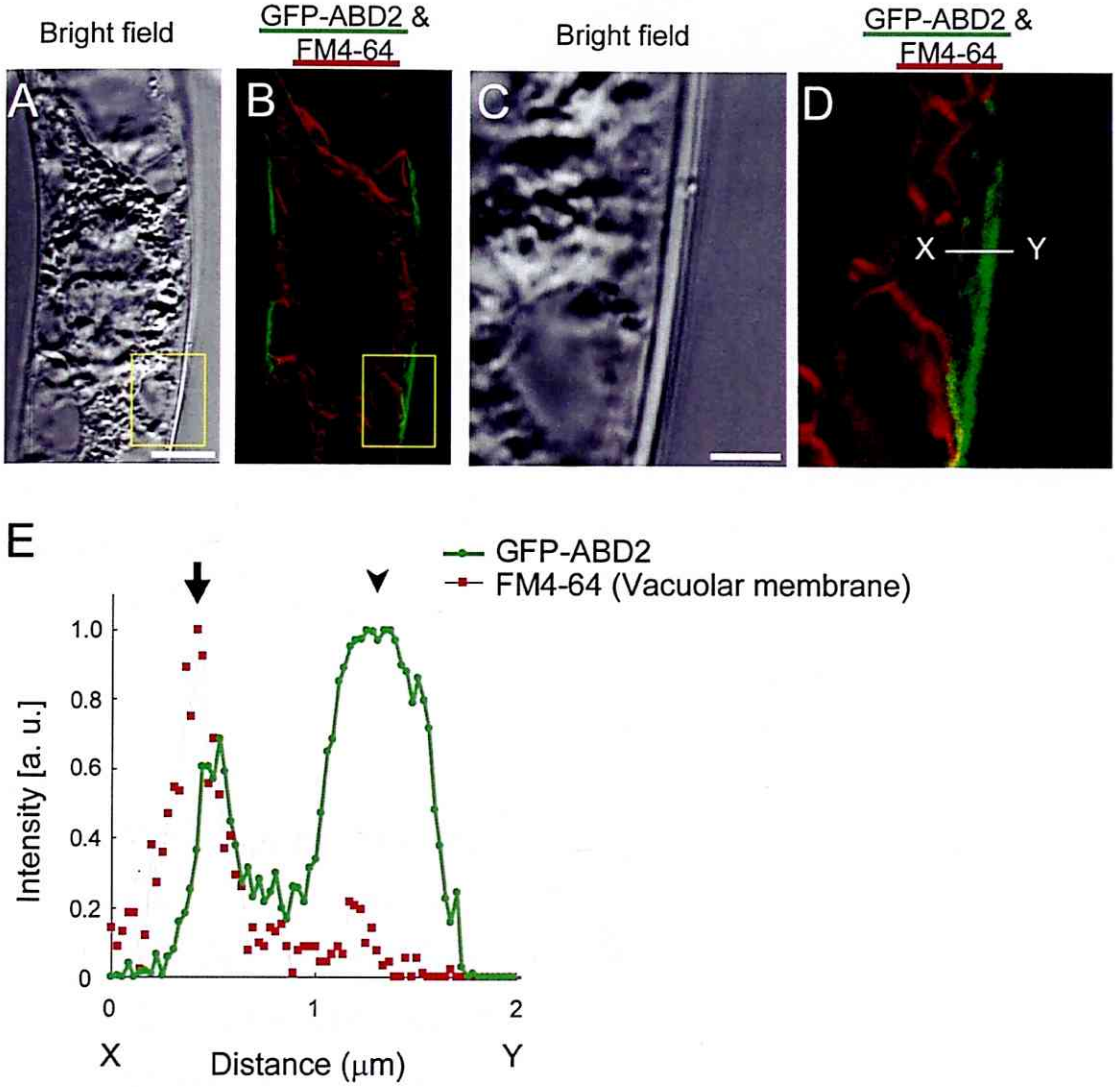

Figure I-3. Double staining of MFs and vacuolar membranes in a mitotic BY-GF11 cell stained with a fluorescent dye, FM4-64. A BY-GF11 cell at metaphase was observed in bright field (A), and by GFP-ABD2 (B, green) and FM4-64 (B, red). (C, D) Magnified images of the boxed region in (A) and (B). (H) An intensity profile of GFP fluorescence and FM4-64 along the X-Y axis in (D). An arrow and arrowhead indicates FM4-64 signal of the vacuolar membrane (VM) and GFP-ABD2 signal on the plasma membrane (PM), respectively.

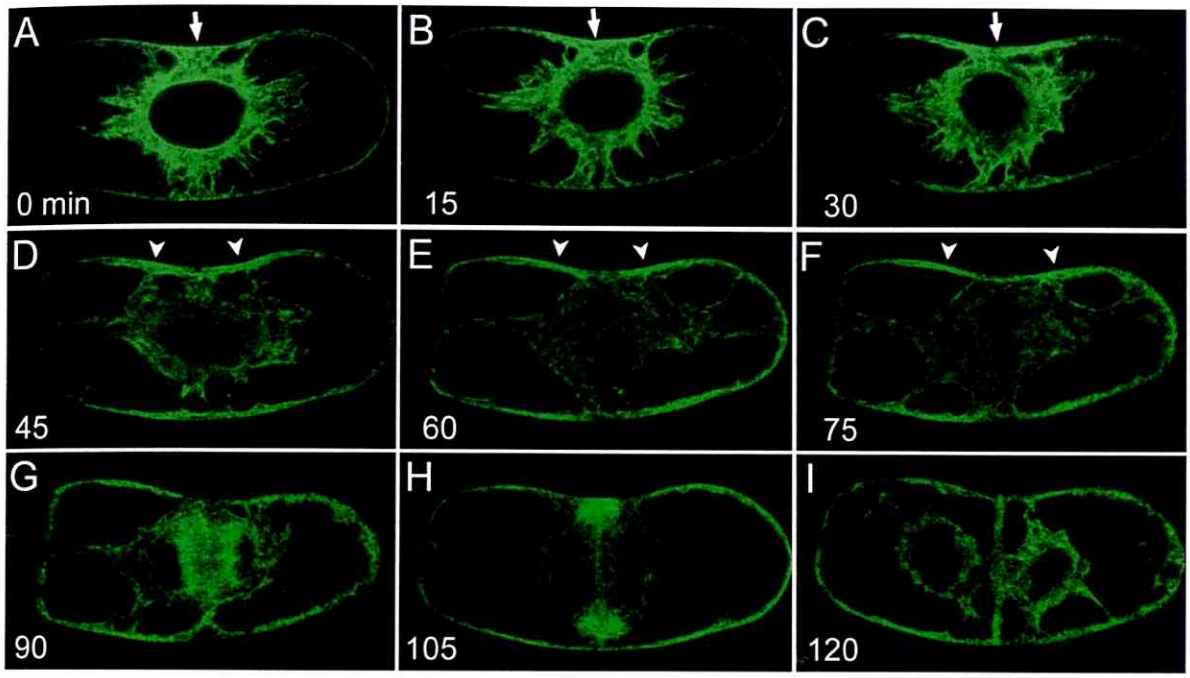

Figure I-4. Time-sequential observations of MFs from late G2 phase to cytokinesis at the mid-plane. In a living BY-GF11 cell, MF structures were observed time-sequentially from late G2 phase (A, 0 min) at 15-min intervals. The cell cycle progressed to the pro- (B, 15 min); prometa- (C, D, 30, 45 min), meta- (E, F, 60, 75 min), ana- (G, 90 min), telo- (H, 105 min) and early G1 (I, 120 min) phases. (A, B, C) Arrows show centre of cortical MF band; (D, E, F) arrowheads show the two MF bands that appeared at the cell cortex. Scale bar: 10 μm.

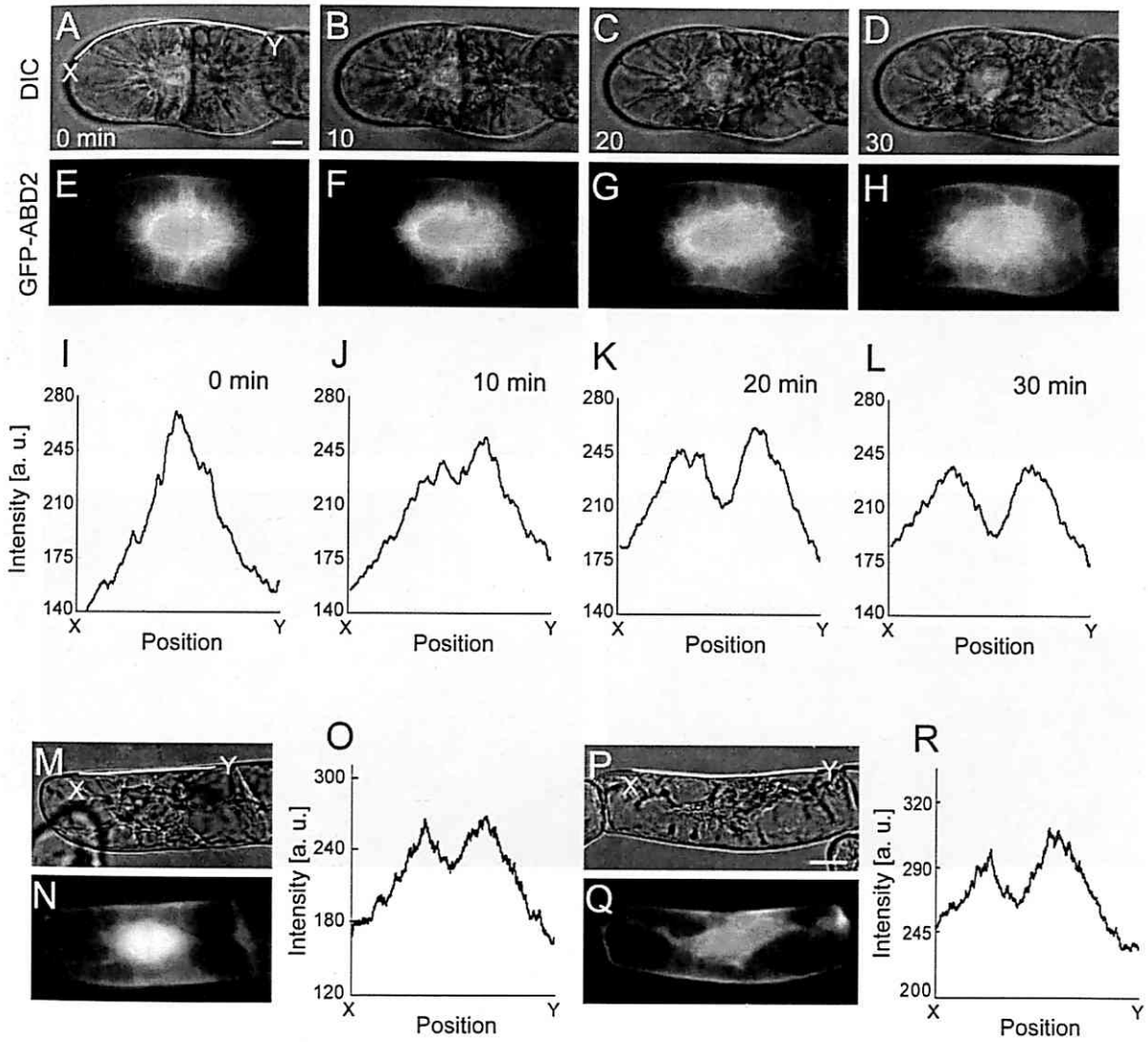

Figure I-5. Rearrangement of cortical MFs from late G2 to metaphase. DIC images (A, B, C, D) and MF structures (E, F, G, H) in a BY-GF11 cell from late G2 phase (0 min) to mitosis (10-30 min). Scale bar: 10 μm. (I, J, K, L) Fluorescent intensities obtained from images of (E, H) at position X-Y in (A). MF twin peaks (MFTP) structure observed in BY-GF8 cells (M, N, O), and BY-2 cells incubated with rhodamine-phalloidin after permeabilization (P, Q, R). DIC images (M, P); MF structures (N, Q); and fluorescent intensities (O, R) obtained from images of (N, Q) at position X-Y in (M, P), respectively.

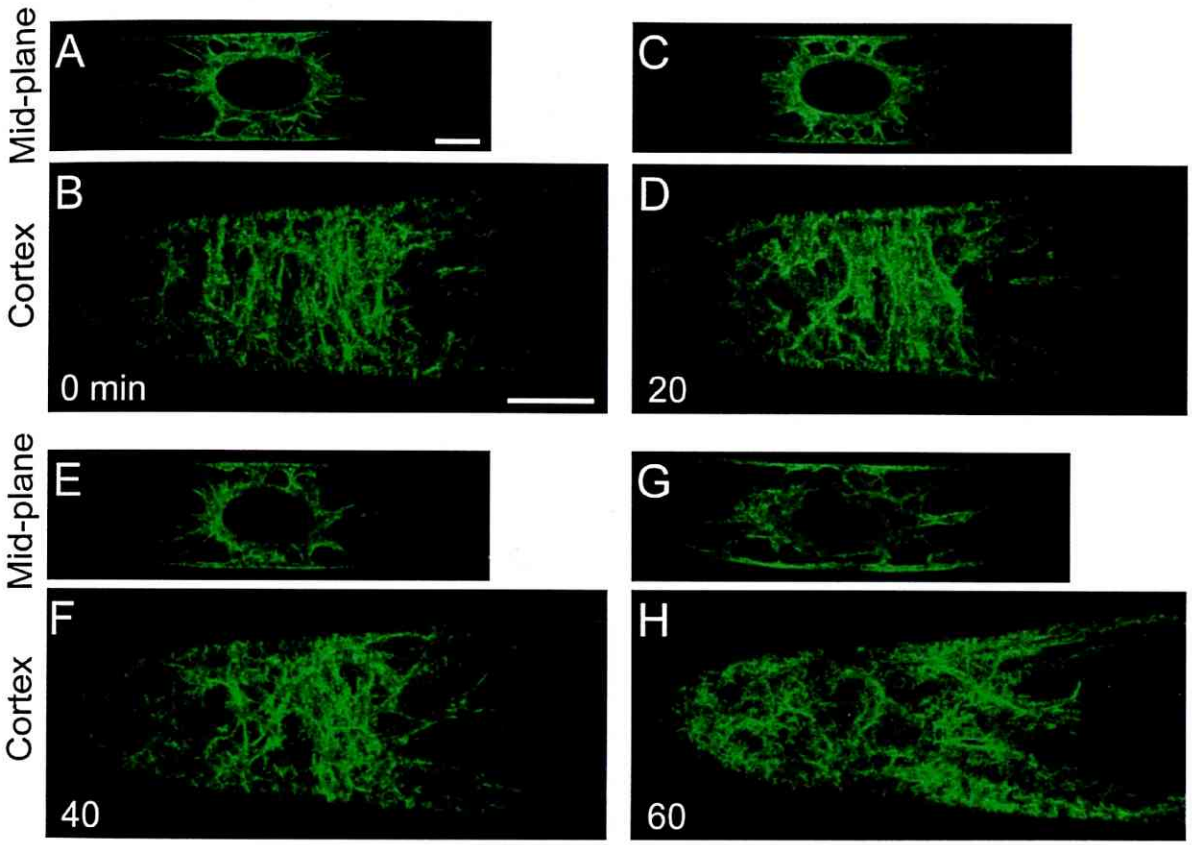

Figure I-6. Time-sequential observations of MFs from late G2 phase to metaphase at mid-plane and cell cortex in a BY-GF11 cell. Images taken from late G2 phase (A, B, 0 min) at 20-min intervals. At 60 min after late G2 phase, the cell cycle progressed to metaphase (G) and formed two MF bands with a weak MF network region (H). Scale bar: 10 μm.

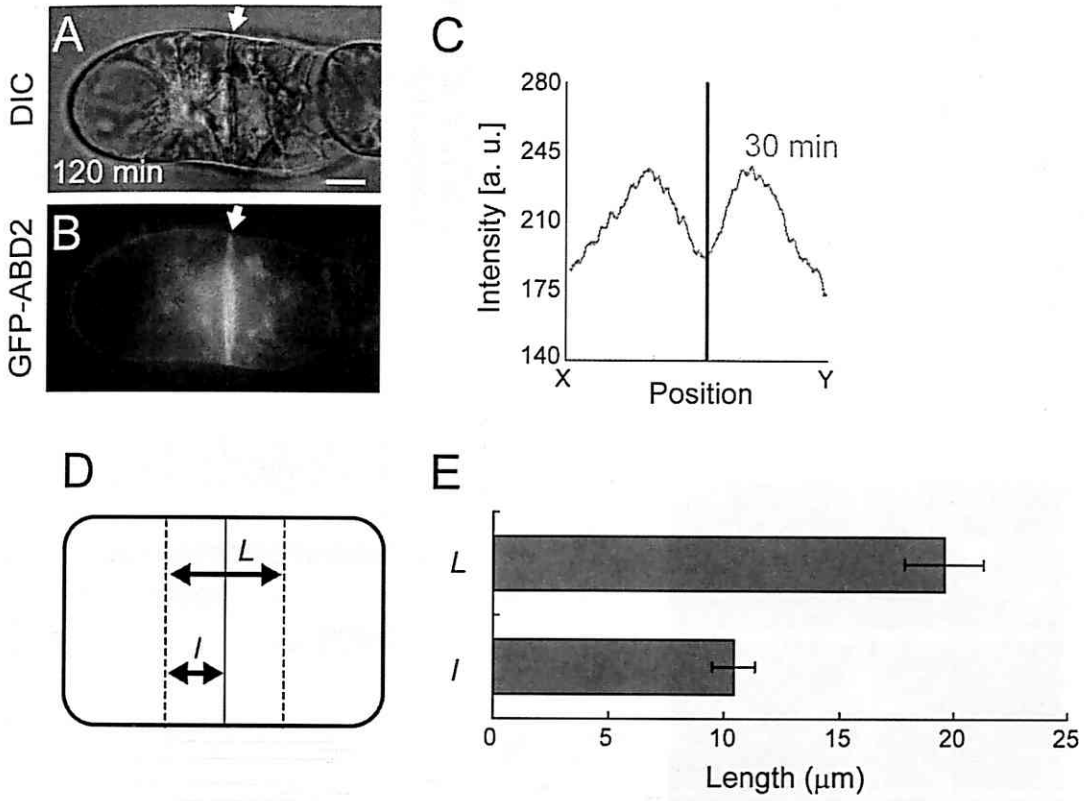

Figure I-7. Positional relationship between division plane and microfilament twin peaks (MFTP). (A, B) DIC image and MF structures at cytokinesis obtained from the cell shown in Figure I-5. Arrows indicate site of cell plate. Scale bar: 10 μm. (C) Comparison of positions of the division plane (A, vertical bar) and MFTP (grey line) observed in Figure I-5L. (D, E) Measurement of distance between two peaks of MFTP (*L*), and that between one peak and the division plane (*l*). Dashed lines and solid vertical line in (D) show positions of MFTP peaks and cell plate, respectively. Data in (E) are mean values ± SE for 10 independent cells. Note that *l* is almost the half the distance of *L*.

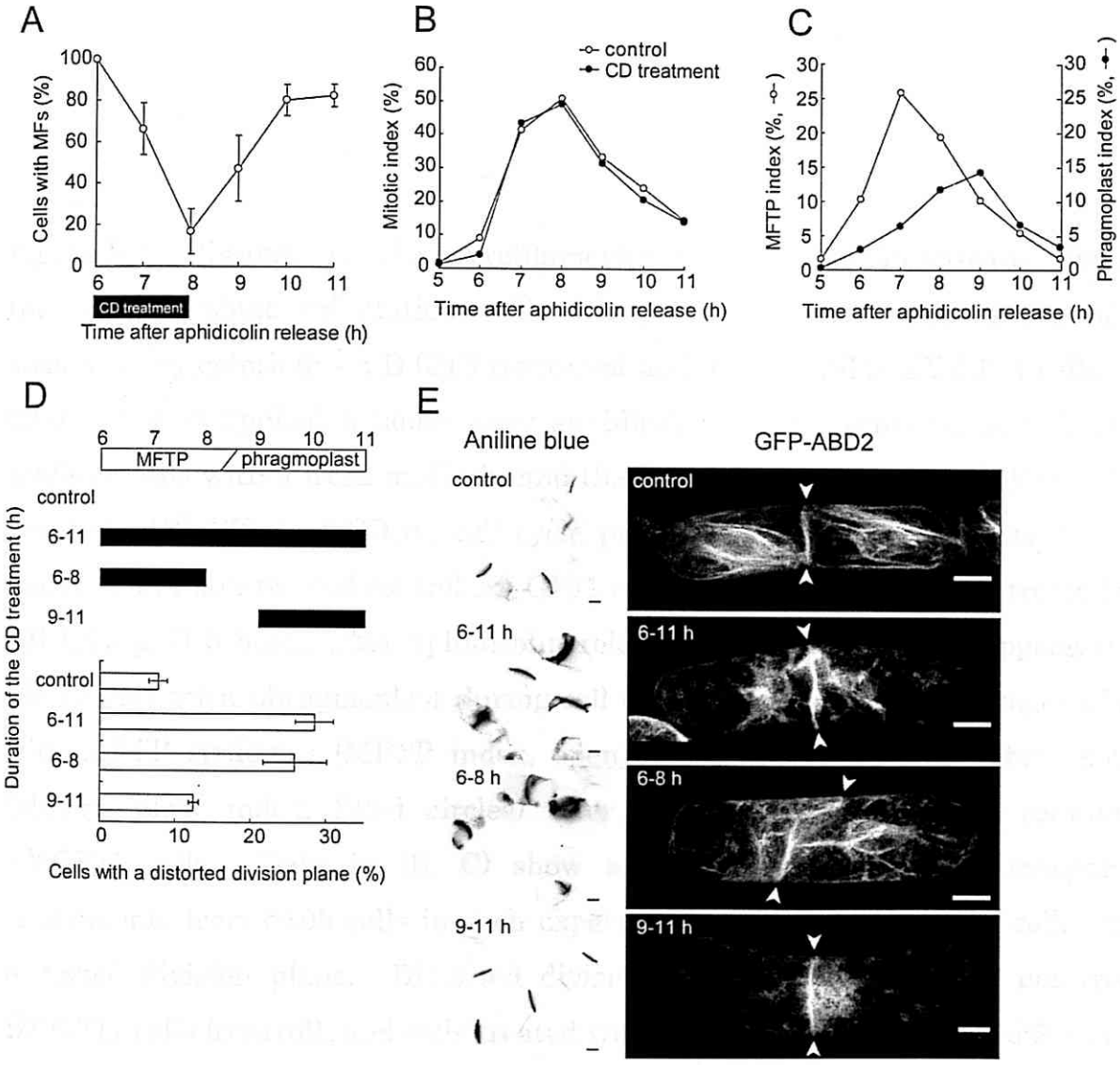
A
Cells with MFs (%)
CD treatment
Time after aphidicolin release (h)
B
control
CD treatment
Mitotic index (%)
Time after aphidicolin release (h)
C
MFTP index (%)
Phragmoplast index (%)
Time after aphidicolin release (h)
D
MFTP
phragmoplast
control
6-11
6-8
9-11
Duration of the CD treatment (h)
Cells with a distorted division plane (%)
E
Aniline blue
GFP-ABD2
control
6-11 h
6-8 h
9-11 h

Figure I-8. Disruption of the microfilament twin peaks (MFTP) structure distorted the division plane orientation. (A) Disappearance and reappearance of MF structures by cytochalasin D (CD) treatment and its removal in BY-GF11 cells. CD (100 μM) was applied 6 hours after aphidicolin release, removed at 8 hours by washing cells with a fresh medium, and the percentage of cells with MF structures counted. (B) Effect of CD on cell cycle progression. Cell cycle progression was monitored in non-treated control BF-GF11 cells (open circles) and cells treated with CD (100 μM) 6 hours after aphidicolin release (filled circles). (C) Appearance of MFTP and actin phragmoplast during cell cycle progression. Percentages of cells with MFTP structure (MFTP index, open circles) and with actin phragmoplast (phragmoplast index, filled circles) after aphidicolin release were counted in BY-GF11 cells. Data in (B, C) show a representative of three independent experiments from >300 cells in each experiment. (D) Percentages of cells with a distorted division plane. Distorted division plane were counted in non-treated BY-GF11 cells (control), and cells treated with CD (100 μM) from 6-11, 6-8 and 9-11 hours after aphidicolin release. Filled bars, duration of CD treatment. Distorted division planes were observed by aniline blue staining 11 hours after aphidicolin release in which the cell cycle was progressed to G1 phase in control cells. Data in (A, D) show mean ± SE of three independent experiments from >300 cells in each experiment. (E) Images of division planes observed by aniline blue staining (left columns) and MF structures (right columns) 11 hours after aphidicolin release in BY-GF11 cells. Conditions of CD treatment as in (D). Arrowheads in images of GFP-ABD2 show division planes. Scale bar: 10 μm.

Chapter II: Cell plate formation

Abstract

In this chapter, time-sequential changes in distribution of actin microfilaments (MFs) were monitored during cytokinesis by live imaging of BY-GF11 cells, which vitally co-stained with the endocytic tracer, FM4-64, that labels the cell plate. During cytokinesis, MFs accumulated near the newly-separated daughter nuclei towards the emerging cell plate, and subsequently approached the expanding cell plate edges. Treatment with an actin polymerization inhibitor caused a decrease in the cell plate expansion rate, which was quantified using live cell imaging and regression analysis. My results demonstrated time-sequential changes in the contribution of MFs to cell plate expansion; MF-disruption caused about a 10% decrease in the cell plate expansion rate at the early phase of cytokinesis, but about 25% at the late phase. MF-disruption also caused malformation of the emerging cell plate at the early phase, indicative of MF involvement in early cell plate formation and expansion. The dynamic movement of endosomes around the cell plate was also inhibited by treatment with an actin polymerization inhibitor and a myosin ATPase inhibitor, respectively. Furthermore, live cell imaging of the endoplasmic reticulum (ER) revealed that MFs were involved in ER accumulation in the phragmoplast at the late phase.

Introduction

Eukaryotic cell division is required for the separation of duplicated chromosomes and the subsequent step of physical division of the mother cells into two daughter cells. In plants, the process of chromosomal separation is generally similar to that of animal cells (Dhonukshe et al. 2006b, Hayashi et al. 2007), whereas the mechanism of physical cell division, called cytokinesis, differs strikingly between plants and animals. In plants, the cell membrane-enveloped juvenile cell wall, referred to as the cell plate, accumulates between the daughter nuclei in late anaphase, and the cell plate subsequently expands centrifugally so as to divide the parental cell into two (Samuels et al. 1995, Dhonukshe et al. 2007). Cell plate formation and expansion are performed by structures that sandwich the developing cell plate, known as the phragmoplast, which is composed of membranes and cytoskeletons.

The cytokinetic membranes are generally thought to originate from Golgi-derived vesicles (Whaley and Mollenhauer 1963, Samuels et al. 1995, Segui-Simarro et al. 2004 Reichardt et al. 2007). During cytokinesis, Golgi stacks were seen to accumulate and to become associated with the cell plate in living tobacco BY-2 cells (Nebenführ et al. 2000) and in cryopreserved shoot apical meristematic cells of *Arabidopsis thaliana* (Segui-Simarro et al. 2006). It was recently proposed that endocytic vesicles also participate in cell plate formation (Dhonukshe et al. 2006a), and this was based on the localization of several cell wall and/or plasma membrane (PM) materials in the cell plate; including xyloglucans (Sonobe et al. 2000, Baluska et al. 2005), pectin (Dhonukshe et al. 2006a, Baluska et al. 2005), PM proteins, such as the auxin transport facilitators, PIN1 (Geldner et al. 2001) and PIN2, the water channel, PIP2, the integral PM protein, LTI6b, and the brassinolide receptor, BRI1 (Dhonukshe et al. 2006a), dynamin (Dhonukshe et al. 2006a), clathrin (Tahara et al. 2007), and the endosomal marker proteins, GNOM-Myc, Ara6 and Ara7 (Dhonukshe et al. 2006a). However, a more recent study demonstrated that endocytosis is not essential for cell plate formation

(Reichardt et al. 2007). The role of endocytosis in cell plate formation thus remains controversial.

Microtubules (MTs) are a major component of the phragmoplast, and the MTs and predicted kinesin motor proteins play a crucial role in the transport of cell plate materials (Mayer and Jürgens 2004, Vanstraelen et al. 2006). The plus-ends of MTs face the cell plate (Euteneuer et al. 1982) and terminate within the cell plate assembly matrix (Segui-Simarro et al. 2004). Recent electron tomographic analysis has revealed, with nano-scale resolution, that the three-dimensional (3-D) geometry of phragmoplast MTs undergoes dynamic changes (Austin et al. 2005).

Actin microfilaments (MFs) are also distributed throughout the phragmoplast and are aligned parallel to the MTs, as reported in endosperm cells of the blood lily, *Haemanthus katherinae* (Schmit and Lambert 1987, Schmit and Lambert 1988, Mole-Bajer et al. 1988, Schmit and Lambert 1990), and the kaffir lily, *Clivia nobilis* (Endle et al. 1998), in root cells of onion, *Allium cepa* (Clayton and Lloyd 1985), in stamen hair cells of spiderwort plants, *Tradescantia virginia* (Cleary et al. 1992, Valster et al. 1997, Valster and Hepler 1997), in cultured cells of carrot, *Daucus carota* (Traas et al. 1987), and alfalfa, *Medicago sativa* (Seagull et al. 1987), as well as in tobacco BY-2 cells (Kakimoto and Shibaoka 1987, Hasezawa et al. 1991). Electron microscopy-based, nano-scale structures of phragmoplast-related MFs have not yet been reported, mainly because of technical limitations (Segui-Simarro et al. 2004). Numerous studies have shown that, unlike MT inhibitors, actin inhibitors could not inhibit the initiation of the cell plate (Valster et al. 1997, Cho and Wick 1990, Mineyuki and Palevitz 1990, Mineyuki and Gunning 1990, Hoshino et al. 2003, this study described in Fig. I-8). However, an actin polymerization inhibitor was found to delay cell plate expansion in *Haemanthus katherinae* endosperm cells (Schmit and Lambert 1987). Microinjection of profilin, a monomeric actin binding protein, into dividing *Tradescantia* stamen hair cells was found to disrupt phragmoplast-associated MFs and to inhibit cell plate expansion (Valster et al. 1997). Furthermore, treatment with 2-3-butanedione monoxime (BDM), an inhibitor of myosin ATPase, or with ML-7, a specific inhibitor of myosin light-chain kinase, could

delay the complete fusion of the cell plate with the parental cell wall (Molchan et al. 2002). Based on these results, MFs have been postulated to contribute to cell plate expansion at the late phase of cytokinesis. However, the mode of MF contribution to plant cytokinesis still remains unclear.

In this study, I have quantitatively estimated the time-sequential changes in MF contribution to cell plate development using live cell image analysis of tobacco BY-2 cell lines. In addition, I examined the relationship between MFs and endomembrane dynamics, including the endosomes and endoplasmic reticulum (ER). My results detail new features of MFs in plant cytokinesis via regulation of the endomembrane system.

Methods

Plant material and synchronization

Cell culture and synchronization of BY-2 cells were performed as described in chapter I. Transgenic BY-2 cell lines expressing a GFP-ABD2 (chapter I, Sano and Higaki et al. 2005, Higaki et al. 2006, Higaki et al. 2007a,b, Higaki et al. 2008) and SP-GFP-HDEL proteins (Mitsuhashi et al. 2000) were previously established.

Microscopy

The cells were transferred into 35-mm-diameter Petri dishes with 14-mm-diameter coverslip windows at the bottom (Matsunami Glass Ind. Ltd, Osaka, Japan). The dishes were placed onto the inverted platform of a fluorescence microscope (IX-70; Olympus) equipped with a CSU10 scanning head (Yokogawa, Tokyo, Japan) and a cooled CCD camera head system (CoolSNAP HQ, PhotoMetricsInc., Huntington Beach, Canada). For multifocal observations, serial optical sections were taken at 0.5-μm intervals. Indirect quantification of fluorescence levels, maximum intensity projections and kymograph construction were performed using ImageJ software (Abramoff et al. 2004).

Cell staining

To observe the cell plate and endosomes, N-(3-triethylammoniumpropyl)-4-(6-(4-(diethylamino) phenyl) hexatrienyl) pyridinium dibromide (FM4-64; Molecular Probes, Invitrogen) was added to the cell suspension at a final concentration of 16 μM. The cells were incubated for 2 min, washed with fresh culture medium, and then monitored. To simultaneously stain the cell plate and callose, the FM4-64-pre-stained cells were fixed with 3.7% (w/v) formaldehyde dissolved in PIPES buffer (pH 6.8) containing 1 mM $MgSO_4$, 5 mM EGTA and 1% glycerol (PMEG) for 1-hour, and then stained with 0.05% aniline blue (Biosupplies Australia, Parkville, Victoria, Australia) in PMEG for 30 min.

Inhibitor

For disruption of MFs, cells were treated with 1 μM bistheonellide A (BA, Wako Pure Chemical Ind., Osaka, Japan) for 60 min before observations. Myosin activity was inhibited by treatment with 20 mM 2-3-butanedione monoxime (BDM, Sigma Chemical Co., St. Louis, MO, USA).

Time-sequential measurements of cell plate diameter

To measure the diameter of an expanding cell plate, a binary image was obtained by intensity thresholding and used for measurements on ImageJ. A Gaussian filter was applied to the cross-sectional images before binarization. Cell plate diameters were calculated with ImageJ software. Regression analysis of the cell plate diameter was performed using Kaleida-graph software (Synergy Software, Reading, PA).

Assessment of cell plate morphology

To assess the cell plate structures, I first obtained cross-sectional images from 70 serial optical sections taken at 0.5-μm intervals of each cell with view orthogonal planes function in MetaMorph image-analysis software (Universal Imaging Co., Downingtown, Panama). Subsequently, I obtained the binary images

from the cross-sectional images by intensity thresholding using ImageJ software as shown in Figure II-5A. To improve the signal to noise ratio, a Gaussian filter was applied to the cross-sectional images before binarization. Cell plate area and perimeter were calculated from the binary images with ImageJ software. Complexity, a secondary morphological parameter, was calculated by $P^2/4\pi A$, where P is the perimeter and A is the area, according to Tanaka et al. (2007).

Analysis of endosomal movement

To estimate the velocity of endosomal movement, I performed time-sequential observations at 1 sec intervals for 30 sec by spinning-disc confocal laser scanning microscopy (CLSM). From the time-sequential images, I measured the distance and time traveled by endosomes using the ImageJ plug-in MTrack2, which was developed for multiple particle detection and tracking, and which is freely available from the website http://valelab.ucsf.edu/~nico/IJplugins/MTrack2.html. Subsequently, endosomal velocity was calculated by dividing the distance traveled by the traveling time.

Results

Dynamic changes in MF localization during plant cytokinesis

To simultaneously observe MFs and the cell plate, tobacco BY-GF11 cells were stained with the styryl dye, FM4-64. After pulse-labeling with this endocytic tracer, the fluorescence moves from the PM to endosomes, and finally reaches the vacuolar membrane (VM) (Kustuna and Hasezawa 2002, Bolte et al. 2004, Samaj et al. 2005; see also chapter I and III.). In addition, FM4-64 localizes to the cell plate membranes of *Arabidopsis* root cells (Dhonukshe et al. 2006a, Dettmer et al. 2006) and tobacco BY-2 cells (Bolte et al. 2004, Mao et al. 2005), in agreement with the previously suggested involvement of the endocytic pathway in membrane trafficking to the cell plate (Dhonukshe et al. 2006a).

From 5 min to 3 hours after pulse-labeling with 16 μM FM4-64, I observed

that the fluorescence became localized mainly in the cell plate membranes and endosomes of the cytokinetic BY-2 cells (Fig. II-1A). At this time, there was still a slight remnant of fluorescence in the PM but not in the VM. For cell plate observations, all results presented in this chapter were, unless otherwise indicated, from those conducted 2 hours after pulse-labeling.

To follow the MF and cell plate dynamics with high-resolution time, I time-sequentially observed the BY-GF11 cells stained with FM4-64 using spinning disc CLSM (Nakano 2002). At metaphase, no prominent MFs or FM4-64 fluorescence was observed in the mitotic apparatus (Fig. II-1A, 0 min), whereas cortical MF twin peaks (MFTP) were evident (Fig. II-1A, 0 min, asterisks). From anaphase to telophase, the FM4-64 fluorescence gradually accumulated at the equatorial region, and the cell plate subsequently emerged (Fig. II-1A, 4-6 min) as previously reported (Dhonukshe et al. 2006a). Concomitantly, there was a gradual accumulation of MFs from the periphery of the daughter nuclei towards the emerging cell plate (Fig. II-1A, 4-6 min). At telophase, the MFs became localized near the expanding cell plate (Fig. II-1A, 8-13 min). Measurements of fluorescent intensity around the division plane illustrate the accumulation of MFs in parallel with development of the FM4-64-labelled cell plate (Fig. II-1B). To evaluate the spatial changes in MFs, a kymograph was constructed by tracking the fluorescence across the developing cell plate (Fig. II-1C). The kymograph suggests that the MFs gradually approached the cell plate (Fig. II-1C, yellow broken lines).

To examine the structural relationship between MFs and cell plate during cytokinesis, the GFP-ABD2 and FM4-64 fluorescent intensities were measured along the cell plate at early (Fig. II-2A, line segment PQ) and late (Fig. II-2F, line segment RS) telophase. GFP-ABD2 was detected all along the equatorial plane, but its intensity was lower than that of FM4-64 in the cell plate at early telophase (Fig. II-2B). In contrast, the intensity of GFP-ABD2 was high, especially at the edges of the cell plate, at late telophase (Fig. II-2G). These results indicate that only a few MFs were localized in the mitotic apparatus at early telophase, but that they accumulated around the expanding cell plate at late telophase. A 3-D

cross-sectional image, reconstructed from serial optical sections, confirmed these localization patterns at early (Fig. II-2C, D, E) and late (Fig. II-2H, I, J) telophase. These results suggest that MFs undergo dynamic changes in their arrangement during cell plate development.

Quantitative analysis of the effects of MF disruption on cell plate expansion

As mentioned above, vital staining with FM4-64 allowed me to follow chromosomal separation (Fig. II-3A, 1-0 min), the gradual accumulation of cell plate vesicles (Fig. II-3A, 1-2 min), cell plate expansion (Fig. II-3A, 3-9 min), and final division of the parental cell (Fig. II-3A, 12 min). To study the role of MFs in cell plate development, these sequential events were monitored under MF-disrupted conditions induced by pre-treatment with the dimeric macrolide, bistheonellide A (BA), an inhibitor of actin polymerization (Saito et al. 1998). Treatment with 1 μM BA for 1-hour almost completely destroyed the MF networks and resulted in the dispersion of free GFP-ABD2 fluorescence in the cytoplasm (Fig. II-3B). A 1-hour pre-treatment with 1 μM BA caused a temporary malformation of the emerging cell plate, which thus appeared to be discontinuous (as described further below; Fig. II-3C, 2 min), and also increased the time needed for the expanding cell plate to complete its fusion with the parental cell wall independently of cell size (Fig. II-3D). These results suggest that MFs partially contribute to cell plate formation and expansion.

To study the time-dependency of MF contribution to cell plate expansion, I sequentially measured the cell plate diameters from time-lapse images. Measurements of cell plate diameter and estimations of cell plate area showed that the expansion rate decreased with time in BA-treated cells (Table II-1, BA treatment), whereas the rate was roughly constant in control cells (Table II-1, control). These results suggest that the contribution of MFs to cell plate expansion increases with the progress of cytokinesis.

To quantitatively estimate this contribution of MFs, I used a simple mathematical model for cell plate expansion, based on the well-known concept of a

constant increase in cell plate area (Gunning 1982). In turn, the diameter increased with the square root of time, as follows:

$$D = a\sqrt{t} \qquad (1)$$

where D is the cell plate diameter, a is the expansion rate, and t is time. The time-lapse data of the diameter fit equation 1 well for the control cells (Fig. II-4A, control) but not for the BA-treated cells (Fig. II-4A, BA treatment), as demonstrated by the chi-square goodness of fit test (Fig. II-4C, model 1). This result suggests that disruption of MFs affected the constancy of cell plate expansion.

Consequently, I developed a new model equation as given by:

$$D = (a - bt^n)\sqrt{t} \qquad (2)$$

where a, b and n are constants. In this model, the expansion rate, $a\text{-}bt^n$, gradually slows if both b and n are positive. In BA-treated cells, the time-lapse data precisely fit this model 2 (Fig. II-4B, BA treatment, Fig. II-4C). The mean values of a, b and n were 6.77, 0.01 and 1.81, respectively (Fig. II-4B, BA treatment). These results indicate that the expansion rate was reduced in BA-treated cells and suggest that MFs make a gradual contribution to cell plate expansion.

However, to compare the contributions of MFs to cell plate expansion in control and BA-treated cells, both data sets need to be applied to the same model equation. When I applied time-lapse data from control cells to model equation 2, n became underspecified because b came close to 0 (data not shown). We, therefore, assumed that n is invariant at 1.81, even in the control cells, and applied the control data to model equation 2 (Fig. II-4B, control). Consequently, the control data precisely fit model 2 as well as model 1 (Fig. II-4C). The mean values of a and b were 7.61 and 0.006, respectively (Fig. II-4B, control). Simulating the expansion rate of the cell plate with model equation 2 quantitatively estimated the changes in the expansion rate (i.e. $a\text{-}bt^n$ in model equation 2) during cytokinesis in control and BA-treated cells (Fig. II-4D). Finally, the contribution of MFs to cell plate expansion could be time-sequentially estimated by the differences between

expansion rates in control and BA-treated cells (Fig. II-4E). The contribution of MFs to cell plate expansion was found to be about 10% just after cell plate formation and gradually increased up to about 25% at the end of cytokinesis (Fig. II-4E).

MF-disruption-induced a temporary malformation of the emerging cell plate

Interestingly, a 1-hour pre-treatment with 1 μM BA caused malformation of the emerging cell plate, which thus appeared discontinuous (Fig. II-3C, 2 min). This aberration was only temporary, in that it could be observed for a maximum of only 1-2 min (Fig. II-3C, 2 min), after which the blank areas of the cell plate were filled in so that it attained a normal appearance (Fig. II-3C, 3-5 min). Cross-sectional images revealed abnormal structures with several holes (Fig. II-5A, upper panels). To assess their morphology, I extracted the cell plate area from the cross-sections (Fig. II-5A, lower panels), and measured their area, perimeter and complexity using ImageJ software (Abramoff et al. 2004). Complexity was defined as a morphological parameter and calculable from the area and perimeter (see Methods) (Tanaka et al. 2007). A circle has the lowest value, 1.0, of complexity and, as the structure becomes more complicated, the complexity reaches appropriately higher values (Tanaka et al. 2007). The mean value of complexity of cell plates in BA-treated cells was higher than that of control cells (Fig. II-5B), whereas their mean areas did not differ significantly (Fig. II-5C). In addition, aniline blue staining revealed that the deformed cell plate contained callose (Fig. II-5D) as in the control cells (data not shown). These results suggest that MFs modulated cell plate formation/expansion at the early phase of cytokinesis, but did not affect callose synthesis.

Actin-myosin-dependent endosomal movement around the cell plate

To investigate the interactive mechanisms of MFs and cell plate formation/expansion, the relationship between MFs and endosomes, which have been implicated in cell plate development (Dhonukshe et al. 2006a), was examined. In a control cell at the late phase, there was active movement of numerous

endosomes (Fig. II-6C, F) around the edge of the expanding cell plate (Fig. II-6A). Some endosomes were found to interact with the edge of the expanding cell plate (Fig. II-6B). To examine the role of actin-myosin systems on endosomal movement around the cell plate, I treated the cells with BA or 2-3-butanedion monoxime (BDM), a general myosin ATPase inhibitor (Samaj et al. 2000, Tominaga et al. 2000). The movements were discernibly inhibited by BA (Fig. II-6D, G) and BDM pre-treatments (Fig. II-6E, H). These inhibitory effects were confirmed statistically by measuring the velocity of the endosomal movements (Fig. II-6I, J, K). Dual observations of MFs and endosomes showed that the endosomes moved towards the cell plate along the MFs (Fig. II-6L, M, N). These results suggest that endosomal movement around the edge of the expanding cell plate depends on the actin-myosin systems.

MF-dependent accumulation of ER in the phragmoplast

To further test the involvement of MFs in endomembrane dynamics during cytokinesis, I analyzed the effects of BA treatment on ER-organization during cytokinesis in tobacco BY-2 cells expressing SP-GFP-HDEL, which is retained within the ER (Mitsuhashi et al. 2000). ER accumulated in the spindle poles in meta-/anaphase (Fig. II-7A, 0-3 min), sandwiched the cell plate in telophase (Fig. II-7A, 6-21 min), and accumulated in the phragmoplast in late telophase (Fig. II-7A, 18-21 min, yellow arrowheads), as previously reported (Segui-Simarro et al. 2004, Nebenführ et al. 2000, Gupton et al. 2006). A 1-hour BA pre-treatment did not induce marked changes in ER-organization at metaphase (Fig. II-7C, 0 min), but did inhibit ER-accumulation in the phragmoplast at late telophase (Fig. II-7C, 48-63 min, yellow arrows). The 3-D images also showed a significant decrease in the amount of ER in the phragmoplast (Fig. II-7B, D). In addition, time-sequential measurements of fluorescent intensity around the division plane illustrated the inhibition of ER-accumulation in the phragmoplast (Fig. II-7E).

Discussion

In this study, I have quantitatively examined the temporary changes in MF contribution to cell plate expansion. To visualize the MFs and cell plate, I used GFP-ABD2 expression and FM4-64 vital staining, respectively. FM4-64, which has been widely used as an endocytosis marker, was found to induce abnormal membrane systems in fungal cells (Torralba and Heath 2002). However, FM4-64 cytotoxicity appears limited in plant cells (Bolte et al. 2004) and, at least under my experimental conditions, abnormal membrane structures or an inhibition of cell division in the BY-2 cells were not observed. The labeling techniques, which cause minimal cell damage, have allowed me to study MF-dynamics and their roles in cell plate development.

MFs contribute to cell plate expansion in late expansion phase, but even in early initiation phase

It is widely accepted that there are two stages in plant cytokinesis that can be distinguished by cell morphological features and sensitivity to caffeine (Valster and Hepler 1997). The first stage is the early initiation phase, which starts immediately after chromosomal separation and involves the deposition and early expansion of the cell plate until it reaches the width of the daughter nuclei. The second stage is the late expansion phase that involves growth of the cell plate beyond the width of the nuclei until it reaches and fuses with the parental cell wall. The late expansion phase is completely inhibited by caffeine (Valster and Hepler 1997), which also inhibits callose deposition and the organization of phragmoplast MTs (Yasuhara 2005).

MFs are thought to be also involved in the late expansion phase of the cell plate. In cytochachalasin-treated *Haemanthus katherinae* endosperm cells, the cell plate often remains incomplete (Schmit and Lambert 1987). Similar cell plate inhibition has been reported in profilin-microinjected *Tradescantia virginiana* stamen hair cells (Valster and Hepler 1997), and in *Tradescantia* stamen hair cells treated with myosin inhibitors (Molchan et al. 2002). In this study, the increase in

MF contribution to the late expansion phase of the cell plate, which was confirmed by time-sequential measurements and data fitting analysis (Fig. II-4), concurs with previous reports and also with the gradual accumulation of MFs near the cell plate found in this study (Fig. II-1C). On the other hand, my results revealed that MF-disruption decreased the expansion rate by about 10%, even just after cell plate formation, but by about 25% at the end of cytokinesis (Fig. II-4E) and, in addition, caused malformation of the emerging cell plate (Fig. II-5). These results suggest that MFs not only facilitate cell plate expansion in the late expansion phase but also in the early initiation phase.

Furthermore, MF-disruption-induced malformation of the cell plate suggests that MFs regulate the early disc-like morphology of the cell plate. In the early phase, the MFs had not yet accumulated near the cell plate, but a thin, widely-spread MF-meshwork could be observed in the mitotic apparatus and near the cell plate (Fig. II-1A, Fig. II-2A, B, C, D, E). The existence of MFs near the cell plate in the early phase was also observed by rhodamine-phalloidin staining of fixed cells of onion *Allium cepa* (Clayton and Lloyd 1985). BA-induced cell plate malformation is reminiscent of the mini-phragmoplasts, which appear during *Arabidopsis* endosperm cellularization (Otegui and Staehelin 2000, Otegui et al. 2001) and in post-meiotic cytokinesis during pollen development (Otegui and Staehelin 2004). Mini-phragmoplasts consist of 2 to12 overlapping MT clusters, assembled between duplicated nuclei, and spaced on average 0.6 μm apart from each other across a given division plane (Otegui and Staehelin 2004). BA-induced cell plate blank regions were approximately of the same size (Fig. II-5A, BA treatment). The fact that similar structures occur by MF-disruption suggests that MFs are involved in the spread and flattening of the cell plate at the early phase.

Actin-myosin system is possibly involved in plant cytokinesis via endosomal dynamics

In this study, I found MF-disruption had parallel, aberrant effects on cell plate development and endosomal movement around the expanding cell plate (Fig. II-6D, G, J). Treatment with the general myosin inhibitor, BDM, revealed that

endosomal movements depended on the actin-myosin system (Fig. II-6E, H, K). MF-dependent endosomal dynamics were also reported in root cells of *Arabidopsis thaliana* (Geldner et al. 2001, Grebe et al. 2003, Ovecka et al. 2005, Kleine-Vehn et al. 2006), *Zea mays* (Balska et al. 2002, Balska et al. 2004), *Medicago truncatula* (Voigt et al. 2005) and pollen tubes of *Picea meyeri* (Chen et al. 2007). Endosome association with MFs was observed in cytokinetic BY-2 cells (Fig. II-6L, M, N) as well as in root hair cells (Voigt et al. 2005). From these results, I hypothesize that the actin-myosin systems are partially involved in endocytic membrane traffic to the cell plate. This notion is supported by recent studies demonstrating that the plant myosin class VIII, ATM1, is localized in the expanding cell plate of tobacco BY-2 cells (Van Damme et al. 2004) and in FM4-64-labelled endosomes of *Nicotiana* benthamiana leaves (Golomb et al. 2008). Although the endocytic pathway might participate in membrane trafficking to the cell plate (Dhonukshe et al. 2006a), it is not essential for completion of cytokinesis (Reichardt et al. 2007). Indeed, as Golgi-derived vesicles transported by MTs and unidentified kinesins are necessary and sufficient for cell plate development (Reichardt et al. 2007, Mayer and Jügens 2004), the contribution of MFs to cell plate formation and expansion may be rather limited. Unfortunately, I could not examine the effects of BDM on cell plate expansion, because BDM-pretreatment inhibited cell division in the BY-2 cells (data not shown), possibly through their side effects on MTs (Samaj et al. 2000). Future studies, using combinations of genetic inhibition of myosin activity and time-sequential morphometry as shown in this study, will reveal the changes in contribution of myosins to cell plate expansion.

MFs regulate ER-accumulation in the phragmoplast at late expansion phase

The ER is one of the first organelles to be visualized during plant cytokinesis. Numerous electron microscopic studies have shown that the tubular ER is first arranged parallel to the spindle MTs in metaphase, and then gradually accumulates near the cell plate and phragmoplast region (Hepler 1982, Hepler and Wolniak 1984, Segui-Simarro et al. 2004). Recent studies on the expression of ER-targeted

fluorescence proteins have further described the dynamic behavior of the ER in living cells (Nebenführ et al. 2000, Gupton et al. 2006). Generally, the complex cortical ER-network structures are found to depend on MFs in plant cells (Boevink et al. 1998, Runions et al. 2006) but on MTs in animal cells (Klopfenstein et al. 1998, Waterman-Storer and Salmon 1998). On the other hand, ER-organization in mitotic spindles is associated mainly with MTs rather than MFs in mitotic cells of the gymnosperms, *Pinus brutia* and *Pinus nigra* (Zachariadis et al. 2003), and in tobacco NT-1 cells (Gupton et al. 2006). My observation that the tubular ER aligned with mitotic spindles in BA-treated cells (Fig. II-7C, 0 min) supports these earlier reports. In addition, I found that BA treatment inhibited ER-accumulation in the phragmoplast, especially in the late expansion phase (Fig. II-7C, 48-63 min, D, E), suggesting that MFs are tightly associated with ER recruitment in the phragmoplast. In dividing tobacco mesophyll protoplasts, an unbiased ER redistribution was also found to be dependent on MFs (Sheahan et al. 2004).

The ER has been implicated in the control of the cytosolic calcium ion concentrations (Hepler 1994) and in facilitation of membrane exchange between the ER and cell plate during cell plate maturation (Segui-Simarro et al. 2004). Therefore, it is likely that MFs contribute to cell plate expansion via recruitment of ER into the phragmoplast, and this is supported by the observed increase in MF contribution at the late phase. Taken together with the results from endosomal dynamics, these findings thus imply that MFs have multiple functions in the endomembrane systems during cytokinesis. Future studies will need to focus on molecular dissection of the complicated interactions between MFs and endomembranes to gain further insights into MF contribution to plant cytokinesis.

References

Abramoff MD, Magelhaes PJ, Ram SJ. (2004) Image processing with ImageJ. *Biophoto. Int.* 11:36-42.

Austin JR, Segui-Simarro JM, Staehelin LA. (2005) Quantitative analysis of changes in spatial distribution and plus-end geometry of microtubules involved in plant-cell cytokinesis. *J. Cell Sci.* 118:3895-3903.

Baluska F, Hlavacka A, Samaj J, Palme K, Robinson DG, Matoh T, McCurdy DW, Menzel D, Volkmann D. (2002) F-actin-dependent endocytosis of cell wall pectins in meristematic root cells. Insights from brefeldin A-induced compartments. *Plant Physiol.* 130:422-431.

Baluska F, Liners F, Hlavacka A, Schlicht M, Van Cutsem P, McCurdy DW, Menzel D. (2005) Cell wall pectins and xyloglucans are internalized into dividing root cells and accumulate within cell plates during cytokinesis. *Protoplasma* 225:141-155.

Baluska F, Samaj J, Hlavacka A, Kendrick-Jones J, Volkmann D. (2004) Actin-dependent fluid-phase endocytosis in inner cortex. *J. Exp. Bot.* 55:463-473.

Boevink P, Oparka K, Santa Cruz S, Martin B, Betteridge A, Hawes C. (1998) Stacks on tracks: the plant Golgi apparatus traffics on an actin/ER network. *Plant J.* 15:441-447.

Bolte S, Talbot C, Boutte Y, Catrice O, Read ND, Satiat-Jeunemaitre B. (2004) FM-dyes as experimental probes for dissecting vesicle trafficking in living plant cells. *J. Microscopy* 214:159-173.

Chen T, Teng N, Wu X, Wang Y, Tang W, Samaj J, Baluska F, Lin J. (2007) Disruption of actin filaments by latrunculin B affects cell wall construction in *Picea meyeri* pollen tube by disturbing vesicle trafficking. *Plant Cell Physiol.* 48:19-30.

Cho SO, Wick SM. (1990) Distribution and function of actin in the developing stomatal complex of winter rye (*Secale cereale* cv. Puma). *Protoplasma* 157:154-164.

Clayton L, Lloyd CW. (1985) Actin organization during the cell cycle in meristematic

plant cells. *Exp. Cell Res.* 156:231-238.

Cleary AL, Gunning BES, Wasteneys GO, Hepler PK. (1992) Microtubule and F-actin dynamics at the division site in living *Tradescantia* stamen hair cells. *J. Cell Sci.* 103:977-988.

Dhonukshe P, Baluska F, Schlicht M, Hlavacka A, Samaj J, Friml J, Gadella TW Jr. (2006a) Endocytosis of cell surface material mediates cell plate formation during plant cytokinesis. *Dev. Cell* 10:137-50.

Dhonukshe P, Samaj J, Baluska F, Friml J. (2007) A unifying new model of cytokinesis for the dividing plant and animal cells. *Bioessays* 29:371-381.

Dhonukshe P, Vischer N, Gadella TW Jr. (2006b) Contribution of microtubule growth polarity and flux to spindle assembly and functioning in plant cells. *J. Cell Sci.* 119:3193-3205.

Dettmer J, Hong-Hermesdorf A, Stierhof YD, Schumacher K. (2006) Vacuolar H^+-ATPase activity is required for endocytic and secretory trafficking in *Arabidopsis*. *Plant Cell* 18:715-730.

Endle MC, Stoppin V, Lambert AM, Schmit AC. (1998) The growing cell plate of higher plants is a site of both actin assembly and vinculin-like antigen recruitment. *Euro. J. Cell Biol.* 77:10-18.

Euteneuer U, Jackson WT, McIntosh JR. (1982) Polarity of spindle microtubules in *Haemonthus* endosperm. *J. Cell Biol.* 94:644-653.

Geldner N, Friml J, Stierhof YD, Jurgens G, Palme K. (2001) Auxin transport inhibitors block PIN1 cycling and vesicle trafficking. *Nature* 413:425-428.

Golomb L, Abu-Abied M, Belausov E, Sadot E. (2008) Different subcellular localizations and functions of *Arabidopsis* myosin VIII. *BMC Plant Biol.* 8:3.

Grebe M, Xu J, Mobius W, Ueda T, Nakano A, Geuze HJ, Rook MB, Scheres B. (2003) *Arabidopsis* sterol endocytosis involves actin-mediated trafficking via ARA6-positive early endosomes. *Curr. Biol.* 13:1378-1387.

Gunning BES. (1982) The cytokinetic apparatus: Its development and spatial regulation. *In The cytoskeleton in plant growth and development.* Edited by: Lloyd CW. London: Academic Press pp.229-292.

Gupton SL, Collings DA, Allen NS. (2006) Endoplasmic reticulum targeted GFP reveals ER organization in tobacco NT-1 cells during cell division. *Plant Physiol. Biochem.* 44(2–3):95-105.

Hayashi T, Sano T, Kutsuna N, Kumagai-Sano F, Hasezawa S. (2007) Contribution of anaphase B to chromosome separation in higher plant cells estimated by image processing. *Plant Cell Physiol.* 48:1509-1513.

Hasezawa S, Marc J, Palevitz BA. (1991) Microtubule reorganization during the cell cycle in synchronized BY-2 tobacco suspensions. *Cell Motil. Cytoskel.* 18:94-106.

Hepler PK. (1982) Endoplasmic reticulum in the formation of the cell plate and plasmodesmata. *Protoplasma* 111:121-133.

Hepler PK, Wolniak SM. (1984) Membranes in the mitotic apparatus: their structure and function. *Int. Rev. Cytol.* 90:169-238.

Hepler PK. (1994) The role of calcium in cell division. *Cell Calcium* 16:322-330.

Higaki T, Goh T, Hayashi T, Kutsuna N, Kadota Y, Hasezawa S, Sano T, Kuchitsu K. (2007) Elicitor-induced cytoskeletal rearrangement relates to vacuolar dynamics and execution of cell death: *in vivo* imaging of hypersensitive cell death in tobacco BY-2 cells. *Plant Cell Physiol.* 48: 1414-1425.

Higaki T, Kutsuna N, Okubo E, Sano T, Hasezawa S. (2006) Actin microfilments regulate vacuolar structures and dynamics: dual observation of actin microfilaments and vacuolar membrane in living tobacco BY-2 cells. *Plant Cell Physiol.* 47: 839-852.

Higaki T, Kutsuna N, Sano T, Hasezawa S. (2008) Quantitative analysis of changes in actin microfilament contribution to cell plate development in plant cytokinesis. *BMC Plant Biol.* 8:80.

Higaki T, Sano T, Hasezawa S. (2007) Actin microfilament dynamics and actin side-binding proteins in plants. *Curr. Opin. Plant Biol.* 10:549-556.

Hoshino H, Yoneda A, Kumagai F, Hasezawa S. (2003) Roles of actin-depleted zone and preprophase band in determining the division site of higher-plant cells, a tobacco BY-2 cell line expressing GFP-tubulin. *Protoplasma* 222:157-165.

Kakimoto T, Shibaoka H. (1987) Actin microfilaments and microtubules in the

preprophase band and phragmoplast of tobacco cells. *Protoplasma* 140:151-156.

Kleine-Vehn J, Dhonukshe P, Swarup R, Bennett M, Friml J. (2006) Subcellular trafficking of the *Arabidopsis* auxin influx carrier AUX1 uses a novel pathway distinct from PIN1. *Plant Cell* 18:3171-3181.

Klopfenstein DRC, Kappeler F, Hauri HP. (1998) A novel direct interaction of endoplasmic reticulum with microtubules. *EMBO J.* 17:6168-6177.

Kutsuna N, Hasezawa S. (2002) Dynamic organization of vacuolar and microtubule structures during cell cycle progression in synchronized tobacco BY-2 cells. *Plant Cell Physiol.* 43:965-973.

Mao G, Chan J, Calder G, Doonan JH, Lloyd CW. (2005) Modulated targeting of GFP-MAP65-1 to central spindle microtubules during division. *Plant J.* 43:469-478.

Mayer U, Jurgens G. (2004) Cytokinesis: lines of division taking shape. *Curr. Opin. Plant Biol.* 7:599-604.

Mineyuki Y, Gunning BES. (1990) A role for preprophase bands of microtubules in maturation of new cell walls, and a general proposal on the function of preprophase band site in cell division in higher plants. *J. Cell Sci.* 97:527-537.

Mineyuki Y, Palevitz BA. (1990) Relationship between preprophase band organization, F-actin and the division site in *Allium*. *J. Cell Sci.* 97:283-295.

Mitsuhashi N, Shimada T, Mano S, Nishimura M, Hara-Nishimura I. (2000) Characterization of organelles in the vacuolar-sorting pathway by visualization with GFP in tobacco BY-2 cells. *Plant Cell Physiol.* 41:993-1001.

Molchan TM, Valster AH, Hepler PK. (2002) Actomyosin promotes cell plate alignment and late lateral expansion in *Tradescantia* stamen hair cells. *Planta* 214:683-693.

Mole-Bajer J, Bajer AS, Inoue S. (1988) Three-dimensional localization and redistribution of F-actin in higher plant mitosis and cell plate formation. *Cell Motil. Cytoskel.* 10:217-228.

Nakano A. (2002) Spinning-disk confocal microscopy: a cutting-edge tool for imaging of membrane traffic. *Cell Struct. Funct.* 27:349-355.

Nebenführ A, Frohlick JA, Staehelin LA. (2000) Redistribution of Golgi stacks and other organelles during mitosis and cytokinesis in plant cells. *Plant Physiol.* 124:135-151.

Otegui MS, Mastronarde DN, Kang BH, Bednarek SY, Staehelin LA. (2001) Three-dimensional analysis of syncytial-type cell plates during endosperm cellularization visualized by high resolution electron tomography. *Plant Cell* 13:2033-2051.

Otegui M, Staehelin LA. (2000) Syncytial-type cell plates: a novel kind of cell plate involved in endosperm cellularization of *Arabidopsis*. *Plant Cell* 12:933-947.

Otegui MS, Staehelin LA. (2004) Electron tomographic analysis of post-meiotic cytokinesis during pollen development in *Arabidopsis* thaliana. *Planta* 218:501-515.

Ovecka M, Lang I, Baluska F, Ismail A, Illes P, Lichtscheidl IK. (2005) Endocytosis and vesicle trafficking during tip growth of root hairs. *Protoplasma* 226:39-54.

Palevitz BA. (1987) Accumulation of F-actin during cytokinesis in *Allum*. Correlation with microtubule distribution and the effects of drugs. *Protoplasma* 141:24-32.

Reichardt I, Stierhof YD, Mayer U, Richter S, Schwarz H, Schumacher K, Jürgens G. (2007) Plant cytokinesis requires de novo secretory trafficking but not endocytosis. *Curr. Biol.* 17:2047-2053.

Runions J, Brach T, Kühner S, Hawes C. (2006) Photoactivation of GFP reveals protein dynamics within the endoplasmic reticulum membrane. *J. Exp. Bot.* 57:43-50.

Saito SY, Watabe S, Ozaki H, Kobayashi M, Suzuki T, Kobayashi H, Fusetani N, Karaki H. (1998) Actin-depolymerizing effect of dimeric macrolides, bistheonellide A and swinholide A. *J. Biochem* 123(4):571-578.

Samaj J, Peter M, Volkmann D, Baluska F. (2000) Effects of myosin ATPase inhibitor 2,3-butanedione 2-monoxime on distributions of myosins, F-actin, microtubules, and cortical endoplasmic reticulum in maize root apices. *Plant Cell Physiol.* 41:571-582.

Samaj J, Read ND, Volkmann D, Menzel D, Baluska F. (2005) The endocytic network

in plants. *Trends Cell Biol.* 15:425-433.

Samuels AL, Giddings TH, Staehelin LA. (1995) Cytokinesis in tobacco BY-2 and root tip cells: a new model of cell plate formation in higher plants. *J. Cell Biol.* 130:1345-1357.

Sano T, Higaki T, Oda Y, Hayashi T, Hasezawa S. (2005) Appearance of actin microfilament 'twin peaks' in mitosis and their function in cell plate formation, as visualized in tobacco BY-2 cells expressing GFP-fimbrin. *Plant J.* 44: 595-605.

Schmit AC, Lambert AM. (1987) Characterization and dynamics of cytoplasmic F-actin in higher plant endosperm cells during interphase, mitosis and cytokinesis. *J. Cell Biol.* 105:2157-2166.

Schmit AC, Lambert AM. (1988) Plant actin filament and microtubule interactions during anaphase-telophase transition: effects of antagonist drugs. *Biol. Cell* 64:309-319.

Schmit AC, Lambert AM. (1990) Microinjected fluorescent phalloidin *in vivo* reveals the F-actin dynamics and assembly in higher plant mitotic cells. *Plant Cell* 2:129-138.

Seagull RW, Falconer MM, Weerdenburg CA. (1987) Microfilaments: Dynamic arrays in higher plant cells. *J. Cell Biol.* 104:995-1004.

Segui-Simarro JM, Austin JR, White EA, Staehelin LA. (2004) Electron tomographic analysis of somatic cell plate formation in meristematic cells of *Arabidopsis* preserved by high-pressure freezing. *Plant Cell* 16:836-856.

Segui-Simarro JM, Staehelin LA. (2006) Cell cycle-dependent changes in Golgi stacks, vacuoles, clathrin-coated vesicles and multivesicular bodies in meristematic cells of *Arabidopsis thaliana*: A quantitative and spatial analysis. *Planta* 223:223-236.

Sheahan MB, Rose RJ, McCurdy DW. (2004) Organelle inheritance in plant cell division: the actin cytoskeleton is required for unbiased inheritance of chloroplasts, mitochondria and endoplasmic reticulum in dividing protoplasts. *Plant J.* 37:379-390.

Sonobe S, Nakayama N, Shimmen T, Sone Y. (2000) Intracellular distribution of

subcellular organelles revealed by antibody against xyloglucan during cell cycle in tobacco BY-2 cells. *Protoplasma* 213:218-227.

Tahara H, Yokota E, Igarashi H, Orii H, Yano M, Sonobe S, Hashimoto T, Hussey PJ, Shimmen T. (2007) Clathrin involved in organization of mitotic spindle and phragmoplast as well as in endocytosis in tobacco cell cultures. *Protoplasma* 230:1-11.

Tanaka Y, Kustuna N, Kanazawa Y, Kondo N, Hasezawa S, Sano T. (2007) Intra-vacuolar reserves of membrane during stomatal closure: The possible role of guard cell vacuoles estimated by 3-D reconstruction. *Plant Cell Physiol.* 48:1159-1169.

Tominaga M, Yokota E, Sonobe S, Shimmen T. (2000) Mechanisms of inhibition of cytoplasmic streaming by a myosin inhibitor 2,3-butanedione monoxime. *Protoplasma* 213:46-54.

Torralba S, Heath IB. (2002) Analysis of three separate probes suggests the absence of endocytosis in *Neurospora crassa* hyphae. *Fungal Genet. Biol.* 37:221-232.

Traas JA, Doonan JH, Rawlins DJ, Shaw PJ, Watts J, Lloyd CW. (1987) An actin network is present in the cytoplasm throughout the cell cycle of carrot cells and associates with the dividing nucleus. *J. Cell Biol.* 105:387-395.

Valster AH, Hepler PK. (1997) Caffeine inhibition of cytokinesis: effect on the phragmoplast cytoskeleton in living *Tradescantia* stamen hair cells. *Protoplasma* 196:155-166.

Valster AH, Pierson ES, Valenta R, Hepler PK, Emons AMC. (1997) Probing the plant actin cytoskeleton and interphase by profilin microinjection. *Plant Cell* 9:1815-1824.

Van Damme D, Bouget FY, Van Poucke K, Inze D, Geelen D. (2004) Molecular dissection of plant cytokinesis and phragmoplast structure: a survey of GFP-tagged proteins. *Plant J.* 40:386-398.

Vanstraelen M, Inze D, Geelen D. (2006) Mitosis-specific kinesins in *Arabidopsis*. *Trends Plant Sci.* 11:167-175.

Voigt B, Timmers AC, Samaj J, Hlavacka A, Ueda T, Preuss M, Nielsen E, Mathur J,

Emans N, Stenmark H, Nakano A, Baluska F, Menzel D. (2005) Actin-based motility of endosomes is linked to the polar tip growth of root hairs. *Euro. J. Cell Biol.* 84:609-621.

Waterman-Storer CM, Salmon ED. (1998) Endoplasmic reticulum membrane tubules are distributed by microtubules in living cells using three distinct mechanisms. *Curr. Biol.* 8:798-806.

Whaley WG, Mollenhauer HH. (1963) Golgi apparatus and cell plate formation: a postulate. *J. Cell Biol.* 17:216-221.

Yasuhara H. (2005) Caffeine inhibits callose deposition in the cell plate and the depolymerization of microtubules in the central region of the phragmoplast. *Plant Cell Physiol.* 46:1083-1092.

Zachariadis M, Quader H, Galatis B, Apostolakos P. (2003) Organization of the endoplasmic reticulum in dividing cells of the gymnosperms Pinus brutia and Pinus nigra, and of the pterophyte *Asplenium nidus*. *Cell Biol. Int.* 27:31-40.

Figures

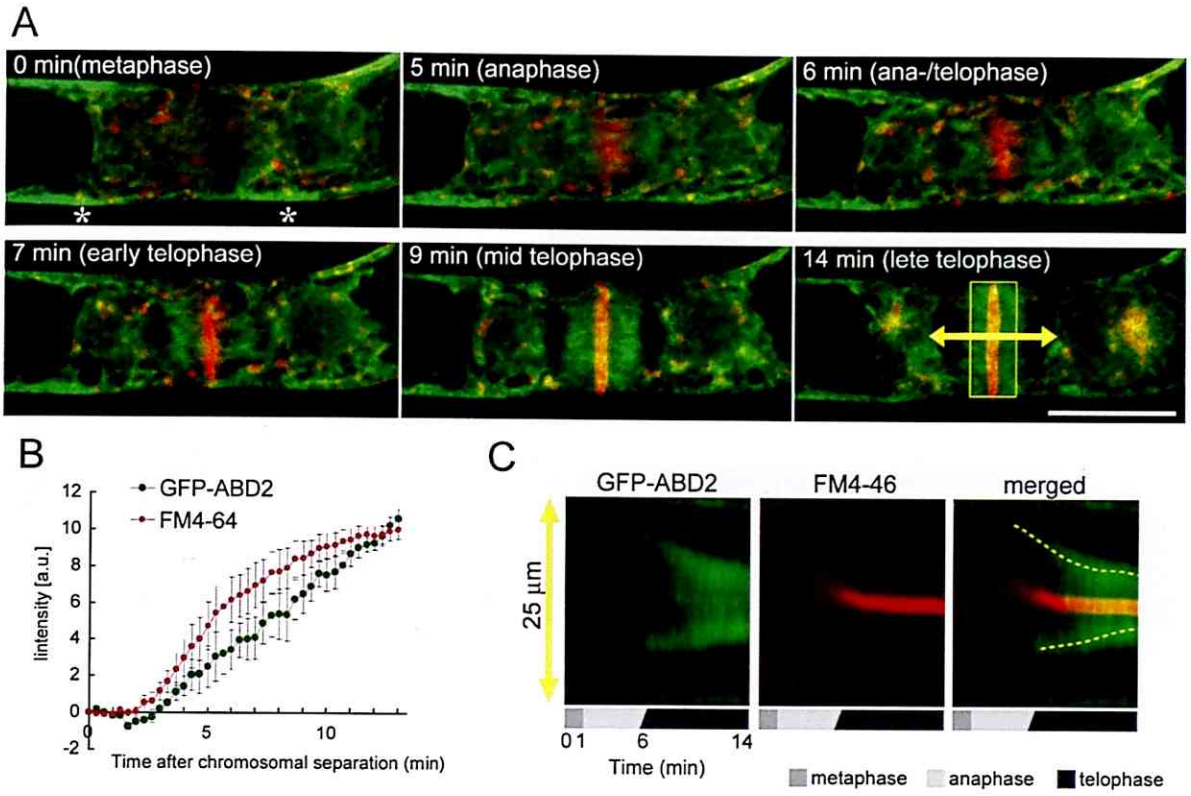

Figure II-1. Time-lapse imaging of actin microfilaments (MFs) and cell plate. (A) Time-lapse images of MFs and FM4-64-stained cell plates from metaphase to late telophase in a BY-GF11 cell. Green and red indicate GFP-ABD2 and FM4-64 fluorescence, respectively. Asterisks indicate actin microfilament twin peaks (MFTP) that appeared at metaphase (see chapter I.). I defined 0 min as the end of metaphase in this figure. Scale bars: 25 µm. (B) Changes in GFP-ABD2 and FM4-64 fluorescence intensities around the division plane. Intensities were time-sequentially measured along the division plane at a width of 9 µm, shown as the boxed region in (A). Data in (B) are mean values ± SE of four independent experiments. (C) Kymographs obtained by drawing a line across a cell plate from metaphase to late telophase, as shown by the yellow arrow in (A). Yellow broken lines indicate changes in MF localization during cell plate development. One representative experiment of four independent experiments is shown.

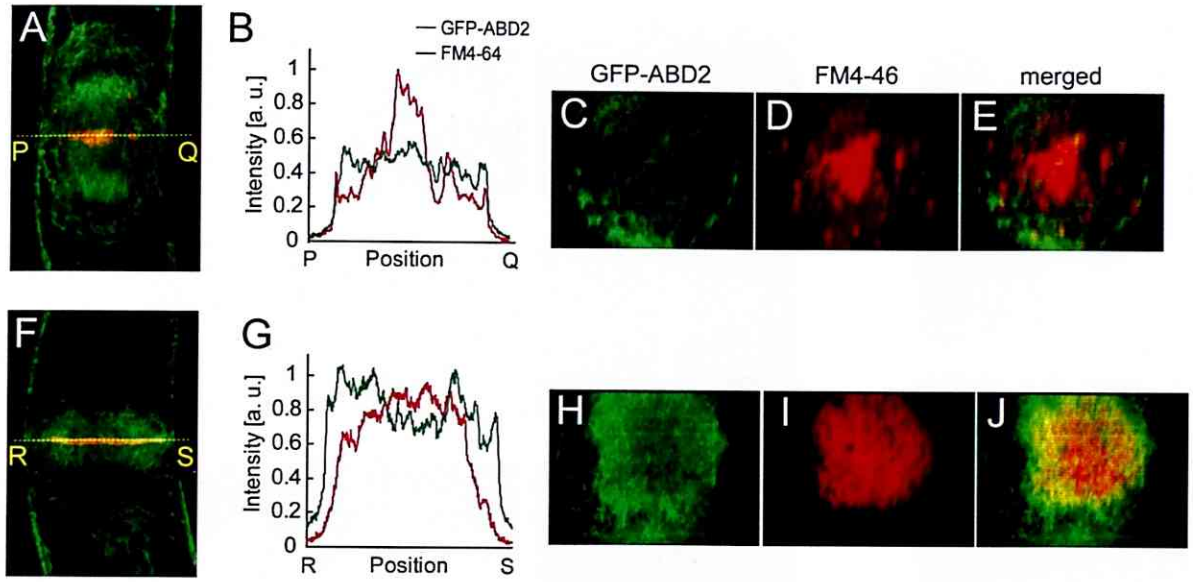

Figure II-2. 3-D localization of MFs at early and late telophase. (A) Single optical section of a BY-GF11 cell at early telophase. Green and red indicate GFP-ABD2 and FM4-64 fluorescence, respectively. (B) Intensity profiles of GFP-ABD2 and FM4-64 along the line segment PQ in (A). (C, D) Cross-sections of GFP-ABD2 (C) and FM4-64 (D) along the line segment PQ in (A). (E) Merged images of (C) and (D). (F) Single optical section of a BY-GF11 cell at late-telophase. Green and red indicate GFP-ABD2 and FM4-64 fluorescence, respectively. (G) Intensity profiles of GFP-ABD2 and FM4-64 along the line segment RS in (F). (H, I) Cross sections of GFP-ABD2 (H) and FM4-64 (I) along the line segment RS in (F). (J) Merged images of (H) and (I). Optical sections, which were used for reconstruction of a cross-section, were taken at 0.5-μm intervals. Scale bars: 10 μm.

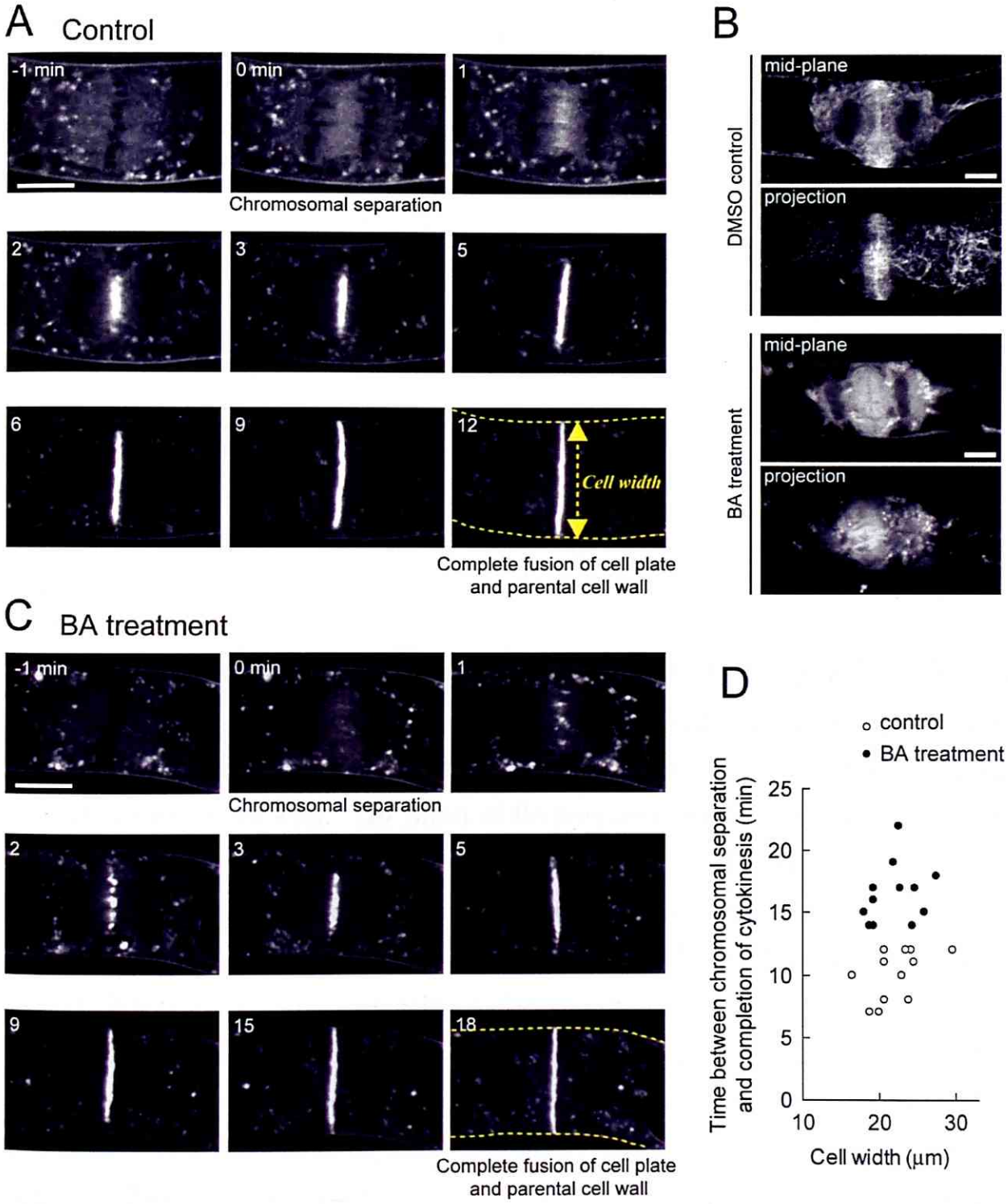
A Control
-1 min
0 min
1
Chromosomal separation
2
3
5
6
9
12
Cell width
Complete fusion of cell plate and parental cell wall
B
DMSO control
mid-plane
projection
BA treatment
mid-plane
projection
C BA treatment
-1 min
0 min
1
Chromosomal separation
2
3
5
9
15
18
Complete fusion of cell plate and parental cell wall
D
control
BA treatment
Time between chromosomal separation and completion of cytokinesis (min)
Cell width (μm)
0
5
10
15
20
25
10
20
30

Figure II-3. Effects of bistheonellide A (BA) on the duration required to complete cytokinesis. (A) Time-lapse images of FM4-64-labelled cell plate expansion in control cells. Time 0 min represents chromosomal separation. Yellow broken lines indicate parental cell wall. (B) Effect of BA treatment on MFs in cytokinetic BY-2 cells. BY-GF11 cells were treated with DMSO or 1 μM BA for 1-hour. Representative images of a single optical section at the mid-plane (mid-plane) and maximum intensity projection (projection) are presented. (C) Time-lapse images of FM4-64-labelled cell plate expansion in BA-treated cells. Time 0 min represents chromosomal separation. Yellow broken lines indicate parental cell wall. (D) Effect of BA treatment on the duration between chromosomal separation and complete fusion of a cell plate and parental cell wall. Note that the duration times in BA-treated cells were longer than those in control cells, and were independent of cell size. The data were obtained from 12 independent experiments of each condition. Scale bar: 10 μm.

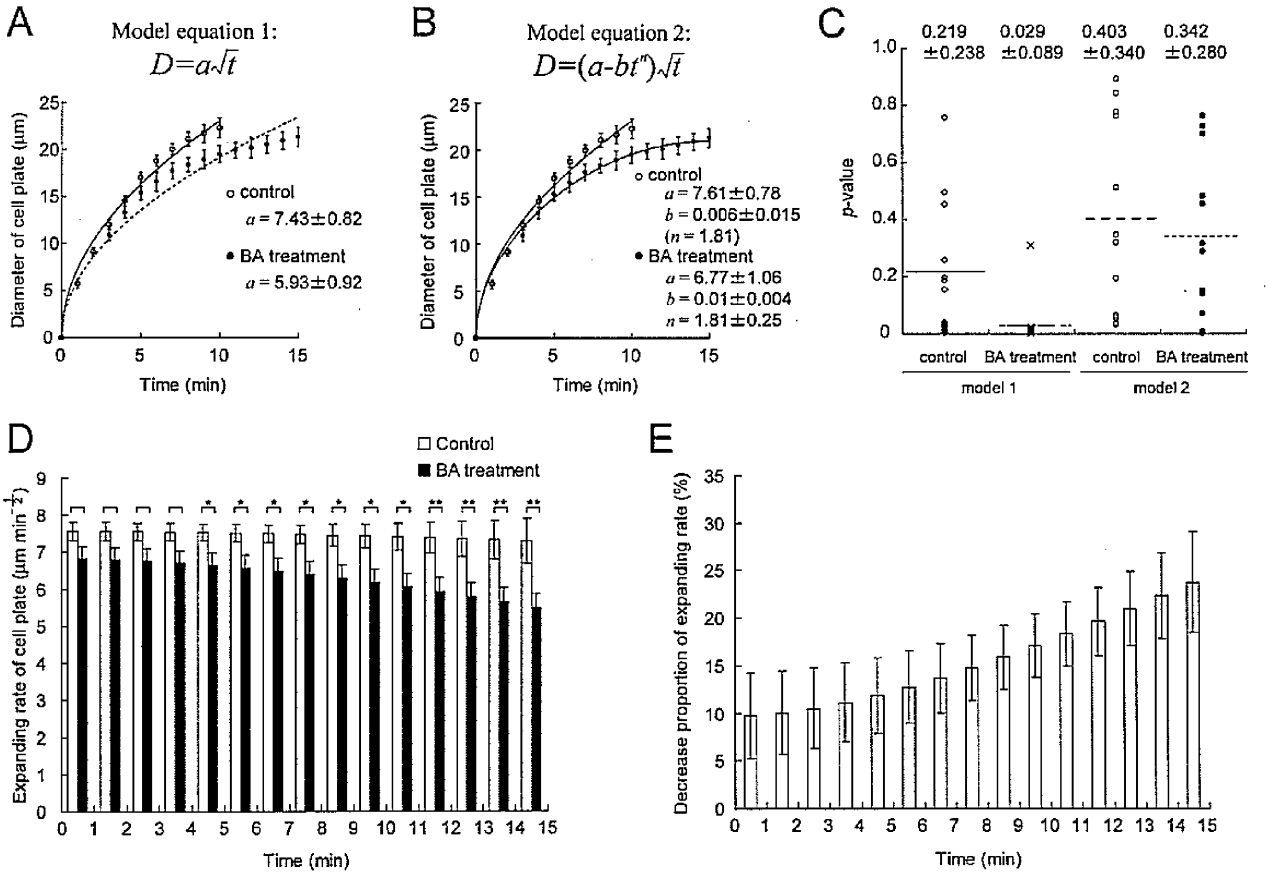
A
Model equation 1:
D=a√t
Diameter of cell plate (μm)
Time (min)
o control
a = 7.43±0.82
• BA treatment
a = 5.93±0.92
B
Model equation 2:
D=(a-bt^n)√t
Diameter of cell plate (μm)
Time (min)
o control
a = 7.61±0.78
b = 0.006±0.015
(n = 1.81)
• BA treatment
a = 6.77±1.06
b = 0.01±0.004
n = 1.81±0.25
C
0.219 ±0.238
0.029 ±0.089
0.403 ±0.340
0.342 ±0.280
p-value
control
BA treatment
control
BA treatment
model 1
model 2
D
□ Control
■ BA treatment
Expanding rate of cell plate (μm min^-1/2)
Time (min)
E
Decrease proportion of expanding rate (%)
Time (min)

Figure II-4. Quantitative analysis of effects of bistheonellide A (BA) on cell plate expansion. (A, B) Regression analysis of the data for changes in cell plate diameter of control (open circle) and BA-treated (filled circle) cells. Time 0 min represents the initiation of cell plate formation. Values are arithmetic means ± SE from 12 independent experiments. The continuous and broken lines represent the regression curves for cell plate diameter of control and BA-treated cells, respectively, calculated from model equation 1 (A) or 2 (B). In model equation 1, the expansion rate a is constant (A). In model equation 2, the expanding rate $a\text{-}bt^n$ undergoes time-dependent changes (B). When the control data was applied to model equation 2, n became underspecified and was consequently assumed to be invariant at 1.81. (C) Comparison of p-values in chi-square goodness of fit tests. The p-value indicates the probability that an observed difference between the measured and predicted values by model equations 1 or 2 occurred by chance alone. If the p-value is less than the significant level at 0.05, I cannot accept that there are no differences between the measured and predicted values. Note that the data fit model equation 2 (B) much better than model equation 1 (A). (D) Simulation of changes in the effects of BA treatment on expansion rate calculated at 1 min intervals. The values are arithmetic means ± SE from 12 independent calculation results of $a\text{-}bt^n$. The 12 parameter sets a and b were the same as calculated in (B). Significance was determined using Student's t-test. p-value *< 0.05. **<0.001. (E) Simulation of changes in the estimated contribution of MFs to cell plate expansion. Values are arithmetic means ± SE from 12 independent calculated results of the decrease proportions of the expanding rate. The decreased proportion was calculated as the ratio of the difference between $a\text{-}bt^n$ in a control and a BA-treated cell to the $a\text{-}bt^n$ in a control cell. The values of $a\text{-}bt^n$ were the same as calculated in (D). Pairing of the control and BA-treated data was performed under the condition that the difference of a in a control and a BA-treated cell was at a minimum value.

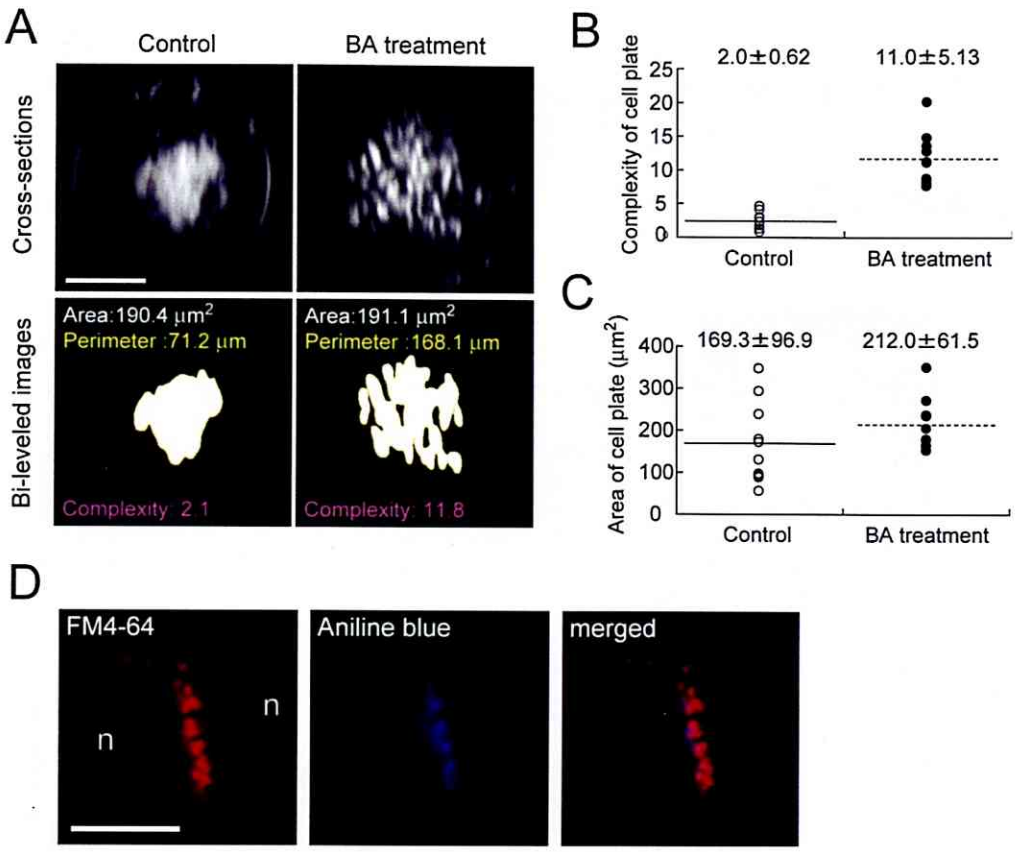

Figure II-5. Effects of bistheonellide A (BA) on morphology of emerging cell plates. (A) Morphometry of cell plates. To define the cell plate configuration from a cross-section (upper images) of an FM4-64-labelled cell plate, a binary image (lower images) was obtained by intensity thresholding. From the binary image, the cell plate area and perimeter were measured. Complexity was calculated from the area and perimeter (see Methods for details). (B, C) Cell plate complexity (B) and area (C). Results from 10 cells in each condition are shown. (D) Double-staining with FM4-64 and aniline blue in fixed cells. n indicates daughter nuclei. Scale bars: 10 μm.

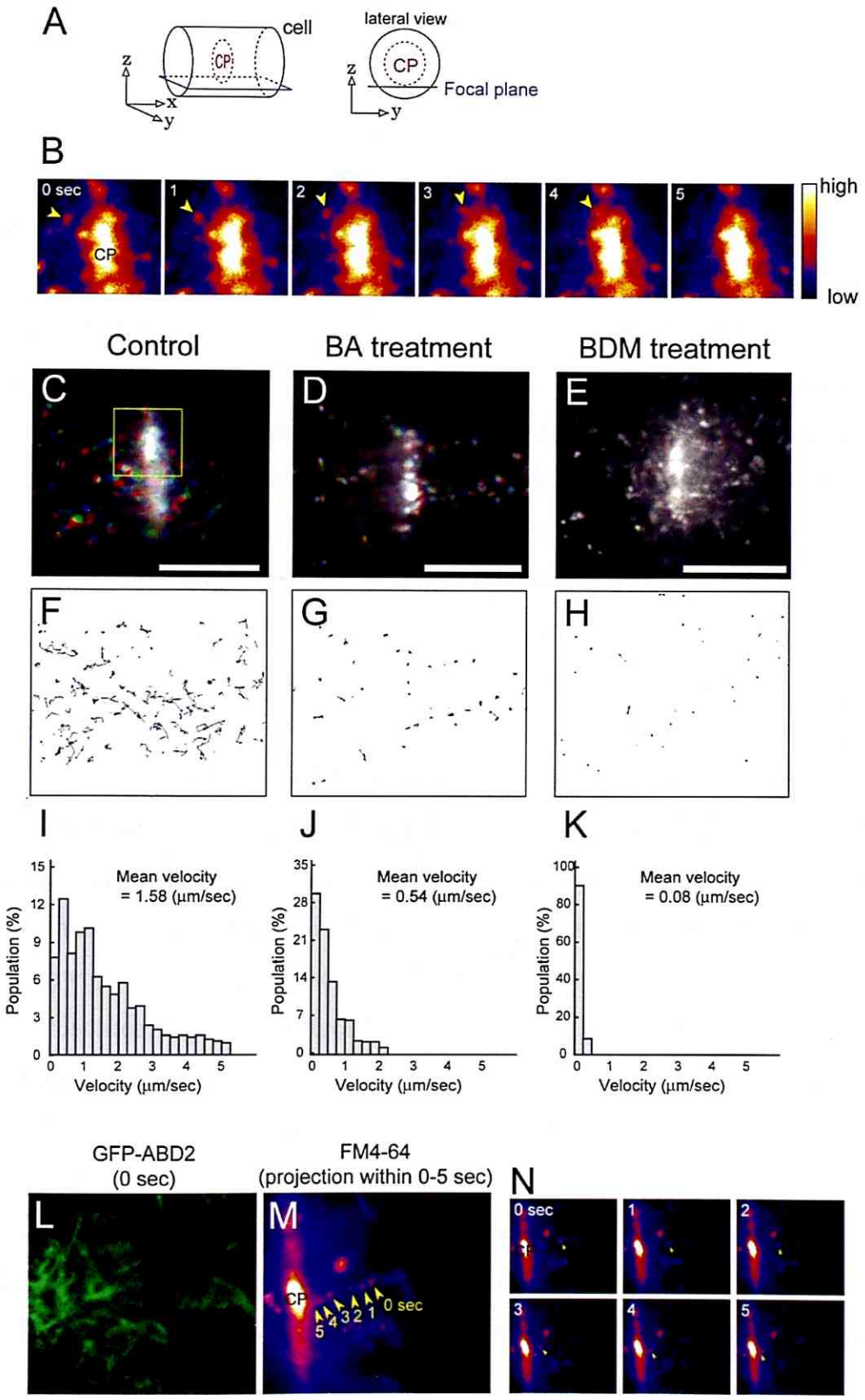
A
cell
CP
z
x
y
lateral view
CP
Focal plane
B
0 sec
1
2
3
4
5
CP
high
low
Control
BA treatment
BDM treatment
C
D
E
F
G
H
I
J
K
Mean velocity
= 1.58 (μm/sec)
Mean velocity
= 0.54 (μm/sec)
Mean velocity
= 0.08 (μm/sec)
Population (%)
Velocity (μm/sec)
GFP-ABD2
(0 sec)
FM4-64
(projection within 0-5 sec)
L
M
N
CP
0 sec

Figure II-6. Effects of bistheonellide A (BA) and 2,3-butanedione monoxime (BDM) on endosome movement around the expanding cell plate edge. (A) Schematic representation of the focal plane for image capture around the edge of an expanding cell plate. All microscopic images presented in this figure were focused at the tangential surface of the cell plate. CP represents the cell plate. (B) Interaction of endosomes with the edge of a cell plate. Magnified and time-sequential images of the boxed region in (C) are shown. To facilitate endosome visualization, images are presented in pseudo-color. Movement of an endosome (yellow arrowheads) towards the cell plate (0-4 sec) and merger with the edge (5 sec). (C-E) Movement of endosomes stained with FM4-64 around a cell plate in control (C), BA-treated (D) and BDM-treated (E) cells. Images at 0, 15 and 30 sec are colored in red, green, and blue, respectively, and projected together. Scale bars: 10 μm. (F-H) Tracking of endosomal movement in control (F), BA-treated (G) and BDM-treated (H) cells. Confocal sections were taken at 1-sec intervals for 30 sec, and the endosomes were tracked by ImageJ software (see Methods for detail.). (I-K) Frequency histograms of endosome velocity over a 30 sec period. Data were obtained from 599 (I), 488 (J), 382 (K) endosomes from 10 control (I), 18 BA-treated (J), and 15 BDM-treated (K) cells, respectively. (L-N) Dual observations of MFs (L) and moving endosomes (M, N). To facilitate endosome visualization, images are presented in pseudo-color as in (B). MF structures around the cell plate edge (L) and endosome movement (N, yellow arrowheads) were observed simultaneously. To facilitate visualization of the movement, maximum intensity projections of the time-sequential images are presented (M). Note the movement of an endosome towards the cell plate along the MFs. CP represents the cell plate. Scale bar: 5 μm.

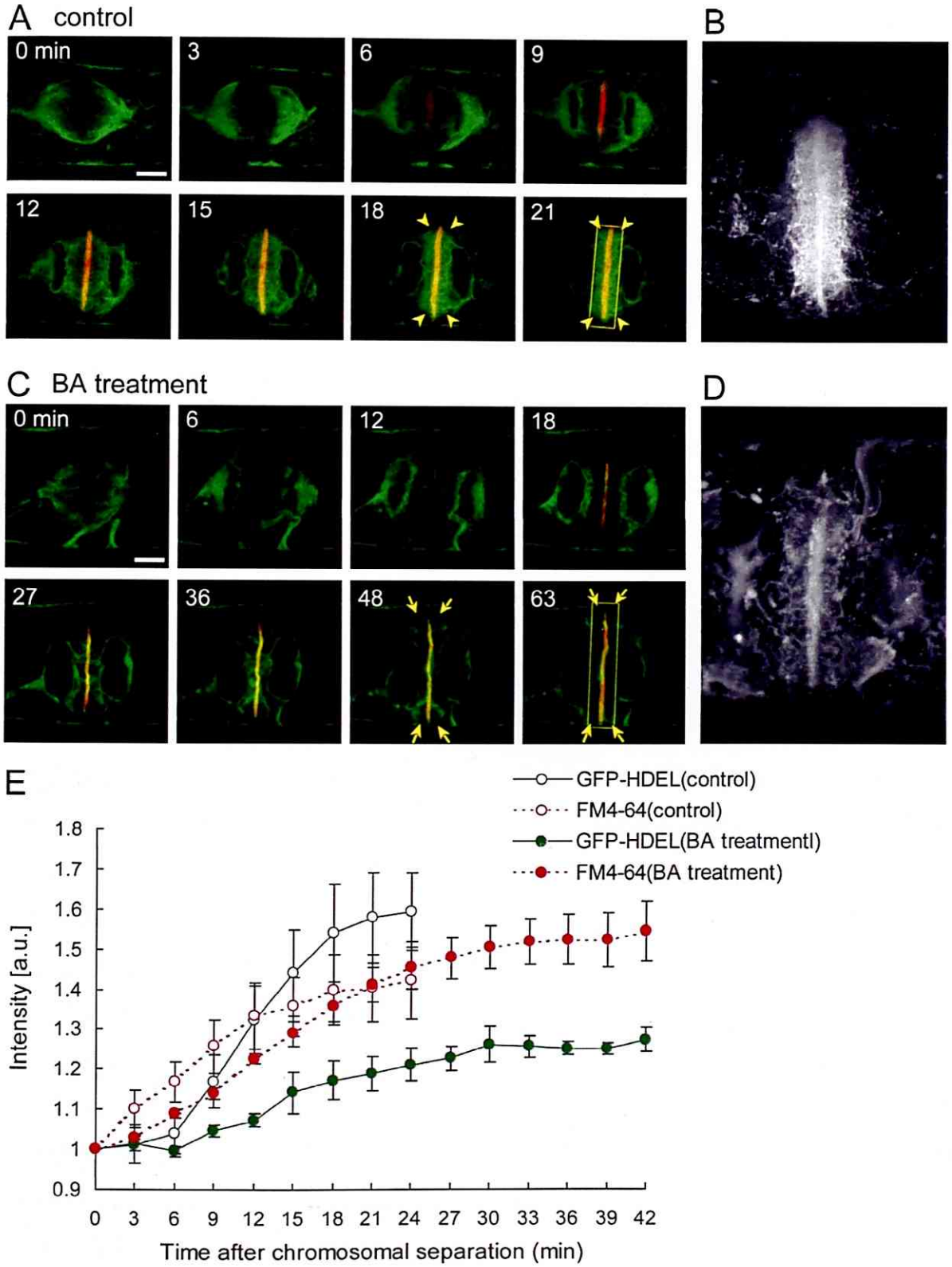
A control
0 min
3
6
9
12
15
18
21
B
C BA treatment
0 min
6
12
18
27
36
48
63
D
E
GFP-HDEL(control)
FM4-64(control)
GFP-HDEL(BA treatmentl)
FM4-64(BA treatment)
Intensity [a.u.]
1.8
1.7
1.6
1.5
1.4
1.3
1.2
1.1
1
0.9
0 3 6 9 12 15 18 21 24 27 30 33 36 39 42
Time after chromosomal separation (min)

Figure II-7. Effects of bistheonellide A (BA) on organization of phragmoplast-related endoplasmic reticulum (ER). (A) Time-lapse images of GFP-labeled endoplasmic reticulum (ER) and FM4-64-labeled cell plate during cytokinesis in a control cell. ER accumulated around the edge of the expanding cell plate before completion of cytokinesis (yellow arrowheads). Scale bar: 10 μm. (B) Projection image of ER at late telophase in a control cell. (C) Time-lapse images of GFP-labeled ER and FM4-64-labeled cell plate in a BA-pretreated cell. Accumulation of ER in the phragmoplast was inhibited (yellow arrows) compared with the control cell shown in (A). Scale bar: 10 μm. (D) Projection image of ER at late telophase in a BA-treated cell. (E) Changes in GFP and FM4-64 fluorescence intensities around the division plane. Intensities were time-sequentially measured in the division plane at a width of 9 μm, as shown in the boxed region of (A) and (C). Data in (E) are mean values ± SEs of four independent experiments.

Table II-1.

Cell plate diameter and estimated cell plate area in tobacco BY-2 cells during cytokinesis.

Time after initiation of cell plate formation (min)	Control			BA treatment		
	Diameter (μm)	Area (μm^2)	ΔArea ($\mu m^2\ min^{-1}$)	Diameter (μm)	Area (μm^2)	ΔArea ($\mu m^2\ min^{-1}$)
0	0	0		0	0	
			37.9 ± 3.6			ND
1	6.9 ± 0.3	37.9 ± 3.4		ND	ND	
			34.3 ± 6.2			ND
2	9.5 ± 0.5	72.2 ± 7.2		ND	ND	
			47.0 ± 6.6			ND
3	12.2 ± 0.5	119.2 ± 10.0		11.2 ± 0.4	99.9 ± 8.2	
			52.9 ± 5.2			49.5 ± 8.1
4	14.7 ± 0.6	172.1 ± 12.7		13.7 ± 0.5	149.4 ± 11.9	
			57.2 ± 5.6			38.2 ±9.4
5	17.0 ± 0.6	229.3 ± 16.9		15.3 ± 0.6	187.5 ± 16.2	
			44.8 ± 6.1			31.5 ± 8.1
6	18.6 ± 0.6	274.0 ± 18.0		16.5 ± 0.8	219.0 ± 20.0	
			39.5 ± 4.6			31.9 ± 4.6
7	19.9 ± 0.6	313.5 ± 18.6		17.7 ± 0.8	251.0 ± 23.0	
			39.0 ± 7.8			19.3 ± 3.9
8	21.1 ± 0.7	352.5 ± 22.9		18.4 ± 0.8	270.3 ± 23.4	
			36.7 ± 7.4			16.9 ± 4.7
9	22.1 ± 0.9	389.2 ± 29.3		18.9 ± 0.8	287.2 ± 24.7	
			38.1 ± 7.7			19.3 ± 5.0
10	22.8 ± 1.0	427.3 ± 24.6		19.6 ± 0.8	306.5 ± 27.1	
						14.5 ± 3.0
11				20.0 ± 0.9	321.0 ± 28.6	
						9.1 ± 1.9
12				20.3 ± 0.9	330.1 ± 29.0	
						11.9 ± 3.0
13				20.7 ± 0.9	342.0 ± 33.6	
						17.1 ± 6.0
14				21.1 ± 1.0	359.1 ± 32.1	
						17.3 ± 7.5
15				21.7 ± 0.9	376.4 ± 32.5	
						7.0 ± 3.4
16				21.9 ± 0.9	383.4 ± 34.3	

ND: Not defined

The diameter of the FM4-64-stained cell plate was measured as shown in Figure II-4A. Values are arithmetic means ±SE, n=12. Cell plate area was estimated by assuming that the cell plate is a perfect circle ($Area = \pi(Diameter)^2/4$). Diameters at 1 and 2 min after initiation of cell plate formation (Table II-1, BA treatment) could not be defined because the emerging cell plate was deformed in BA-treated cells (see Fig. II-3C, 2 min and Fig. II-5).